Development of Method for Measuring the Beta-functions in the MAX IV Laboratory 1.5 and 3 GeV Storage Rings

DAVID K. OLSSON
IN COOPERATION WITH MAX IV LABORATORY
MASTER´S THESIS
DEPARTMENT OF ELECTRICAL AND INFORMATION TECHNOLOGY
FACULTY OF ENGINEERING | LTH | LUND UNIVERSITY

Development of Method for Measuring the Beta-functions in the MAX IV Laboratory 1.5 and 3 GeV Storage Rings

David K. Olsson
david.olsson.do@gmail.com

Department of Electrical and Information Technology
Lund University

Supervisor: Anders Karlsson
Assistant Supervisors: Åke Andersson and Magnus Sjöström

Examiner: Mats Gustafsson

June 16, 2017

LUND
UNIVERSITY

Printed in Sweden
Tryckeriet i E-huset, Lund

Abstract

In any storage ring or synchrotron based light source one of the most important factors for generating light with desirable properties is the electron beam itself. The dynamics of the beam must be properly characterised and, ideally, adjusted to the desired values for the light source to be able to deliver radiation of the quality which was decided during its design.

This thesis is limited to some of the linear beam dynamics of the MAX IV 1.5 GeV storage ring. Before any measurements on the dynamics can be done the position of the beam has to be accurately determined. This is done by modulating the strength of the quadrupoles. The effect the modulation will have on the beam is linear with respect to the beam displacement from the centre of the quadrupole. Using this technique it was possible to determine the beam position with a better reproducibility than assumed during the machine design.

The beta functions of the machine can be measured by fitting the model to measured data using an algorithm called LOCO. The magnet strengths which give a machine more similar to the nominal model are also obtained from the fit. These values can be used to correct manufacturing errors, electrical errors etc. The LOCO algorithm was able to properly characterise the storage ring, but due to a heating problem all corrections could not be done.

An independent measurement method is to measure the beta functions through the modulation of the quadrupoles and the resulting shift in betatron tune. The beta function values found using this technique had a large offset. The method needs further investigation before it can be used reliably.

Acknowledgements

I would like to thank my supervisors: Anders Karlsson for his encouragement, Åke Andersson for the enthusiastic discussions, and Magnus Sjöström for his tireless support and guidance.

I would also like to thank all the people of MAX IV, PhD students and staff, in particular the operators, for all the help and insight during the thesis work. Thank you for letting me do my master's thesis at such a fantastic workplace.

Popular Science Summary

Measurement and Correction of Beam Properties at the MAX IV Laboratory

The particle accelerators which appear in popular media are often of the high energy physics kind, such as the LHC at CERN, Geneve. These machines investigate the fundamental laws of physics through the use of particle collisions at very high energy. A more common type of particle accelerators are the synchrotron light sources. They use a beam of accelerated electrons to generate high intensity light. To ensure that the generated light has the desired properties it is important to be able to properly measure and control the electron beam.

MAX IV is a state-of-the-art laboratory in Lund, Sweden, which was inaugurated in June, 2016. It is a storage ring based synchrotron light source. The facility has two storage rings which use magnets to contain beams of elections travelling in a closed loop at almost the speed of light. These electrons are used to generate soft and hard X-rays at several systematically positioned sections throughout the rings. The X-rays are used as probes for experiments in fields ranging from life sciences to material science and archaeology. As the generated radiation depends highly on the parameters of the electron beam, it is important that these can be accurately measured and controlled.

The transverse position of the electron beam is monitored by *Beam Position Monitors*, or BPMs. They consist of four pin shaped electrodes capable of detecting the position of the electron beam through electromagnetic induction. The BPMs need to be calibrated in order to report the correct values. The calibration makes use of the electron beam itself, and the fact that the magnetic field in the transverse centre of many types of magnets is zero. Changing the strength of such a magnet has no effect on the electron beam that is centred in the magnet. By placing the beam at a few positions in this magnet and modulating its strength, the centre of the magnet relative to the BPM can be calculated.

Two other important electron beam parameters are the horizontal and vertical beta functions. These can essentially be interpreted as a combination of the transverse size and divergence of the beam throughout the circumference of the storage ring. At all the sections in the ring where the desired X-rays are generated, the

beta functions should preferably have the same constant value. The beta functions can be determined by modulating the focusing of the beam and measureing the resulting oscillations of the beam. They can also be found by comparing how the beam in the machine is affected by changes in magnet strength compared to a simulation of the machine. From this simulation the magnet strengths needed to attain the correct beta function values can be calculated.

The calculated values can be used when adjusting magnet strengths in the machine. This yields a machine with a performance closer to the nominal model.

Table of Contents

Chapter 1
Introduction

On the 21th of June 2016, the third generation storage ring based light source MAX IV was inaugurated in Lund, Sweden. It produces soft and hard X-rays with properties which can be controlled with high precision. This radiation is a very useful probe in a vast range of scientific fields, from archaeology to material science. The radiation is emitted by highly relativistic electrons circulating both of the facilities two storage rings. As this radiation is highly dependent on the parameters of the electron beam it is important to be able to both measure and control these parameters.

This thesis work concerns the measuring of beam position monitor offsets, and the measuring and correction of the beta function beat in the 1.5 GeV storage ring. This storage ring was still in installation at the time of the inauguration. At the beginning of this thesis work it was possible to inject and store beam in the ring.

1.1 Aims of Project

The aims of this master thesis project are:

- To find a beam position monitor offset measurement procedure capable of finding offset values with a reproducibility of 3 µm, or less.
- To implement the LOCO-algorithm on the 1.5 GeV storage ring, and use it to correct beta-beat down to $1 - 2$ %.
- To measure the beta function of the 1.5 GeV storage ring using a separate measurement technique.

Chapter 2
Theory

The general theory in this chapter is taken from two main sources: Helmut Wiedemann's *Particle Accelerator Physics*[2], and Klaus Wille's *The Physics of Particle Accelerators, an introduction*[3].

2.1 Synchrotrons and Storage Ring Based Light Sources

The fundamental laws of electrodynamics state that a charged particle emits electromagnetic waves when accelerated. In *synchrotrons* and *storage rings*, where electrons travel at relativistic speeds, this radiation is referred to as *synchrotron radiation*. A synchrotron is a type of cyclic particle accelerator. The electrons in such a machine travel along a fixed close loop, and the radiation occurs when the path is bent by magnetic fields. These fields are also used to focus the electron beam, similar to the way lenses are used to focus a beam of light. As the electrons lose energy when they emit radiation they also need to receive energy, else they will very quickly be lost. The replenishing of energy is typically done by standing electromagnetic waves in specially designed cavities along the electron path.

In order to have a more controlled light emission, so called *insertion devices* are placed along the path of the electrons. These consist of arrays of, usually permanent, magnets of alternating polarity, causing the beam to wiggle back and forth. This allows for radiation with more controlled properties, e.g. wavelength and polarisation.

In a storage ring electrons are kept in a fixed closed loop path. They are inserted after being accelerated to either nominal or less than nominal energy. In the latter case the final energy of the particles is reached in the storage ring itself. The purpose of the storage ring based light source is to have insertion devices generating reliable radiation in a wide spectrum with high reproducibility. Thus it is very important that the characteristics of the ring are well known, and can be controlled.

Historically synchrotron light was an unavoidable loss of energy in accelerators designed with different purposes in mind. When the useful applications of the radiation were made clear, around 1961, the first generation light sources were born. These were sometimes called parasitic facilities, as the main purpose of these were often high energy or nuclear physics. The first dedicated synchrotron radiation facility, The 2 GeV Synchrotron Source (SRS) at Daresbury, England,

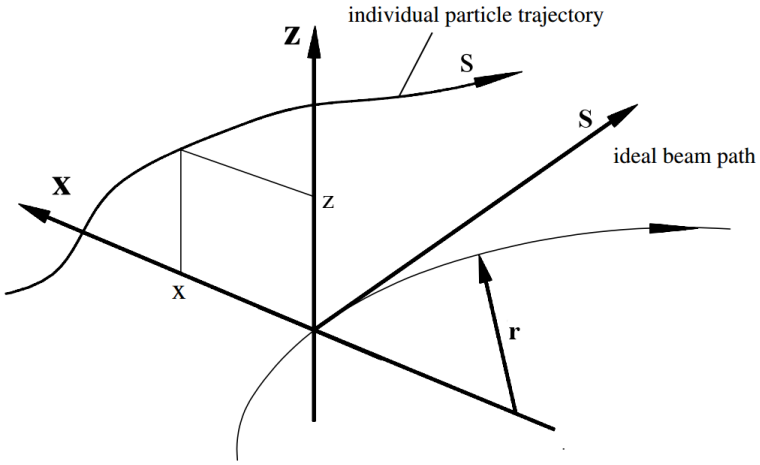

Figure 2.1: Curvilinear coordinate system.[2]

began running experiments in 1984. This was a so-called second generation light source.[1]

With the addition of insertion devices the third generation synchrotron light sources were born. The first facility of this generation to be completed was the European Synchrotron Radiation Facility (ESRF, 6 GeV storage ring) in Grenoble, France, which ran its first experiments in 1994[1]. One of the most recent third generation synchrotron light source facility at the time of writing is the MAX IV Laboratory in Lund Sweden. It comprises of a 3 GeV and a 1.5 GeV storage ring, and an additional short-pulse facility.

2.2 Linear Transverse Beam Optics

2.2.1 Curvilinear Coordinate System

It is possible to describe the beam optics in a strict Cartesian coordinate system. However, this would lead to long and complicated expressions. In order to simplify a so called *Curvilinear* coordinate system is often introduced.

Assume a reference particle moving along the ideal path defined by a structure of different order magnetic fields, often referred to as a *lattice*. Let also an orthogonal coordinate system move along the ideal path of said particle (see Figure 2.1).

We define the coordinate system through the three orthogonal unit vectors:

$$\mathbf{u}_x(s) \equiv -\frac{\mathrm{d}\mathbf{u}_s(s)}{\mathrm{d}s} \Big/ \left|\frac{\mathrm{d}\mathbf{u}_s(s)}{\mathrm{d}s}\right| \qquad \text{Horizontal} \qquad (2.1)$$

$$\mathbf{u}_z(s) \equiv \mathbf{u}_s(s) \times \mathbf{u}_x(s) \qquad \text{Vertical} \qquad (2.2)$$

$$\mathbf{u}_s(s) \equiv \frac{\mathrm{d}\mathbf{r}_0(s)}{\mathrm{d}s} \qquad \text{Longitudinal} \qquad (2.3)$$

where $\mathbf{r}_0(s)$ is the position of the ideal particle in a Cartesian coordinate system for a given longitudinal position s[2].

The coordinate vector $\mathbf{u}_x(s)$ is defined as parallel to the radius of curvature of any circular motion of the beam. As this report will almost exclusively cover storage rings where the path of the ideal beam is only bent in one direction this definition will not cause problems.

Describing particle motion and magnetic fields in a storage ring becomes simpler and more intuitive when using this coordinate system.

2.2.2 The Lorentz Force

A particle with the charge e and the velocity $\mathbf{v}$ travelling through an electromagnetic field experience the *Lorentz force*:

$$\mathbf{F} = e(\mathbf{E} + \mathbf{v} \times \mathbf{B}) = \dot{\mathbf{p}} \qquad (2.4)$$

where $\mathbf{E}$ and $\mathbf{B}$ are the electric and magnetic fields, respectively.

In an electron storage ring we have that $|\mathbf{v}| \approx c$. Thus, for an electric field to have the same effect on the particle as a magnetic field it would need to be stronger by a factor c. Magnetic fields are used to steer the beam in a storage ring since it is much easier to achieve a magnetic field strength of 1 T than an electric field of $3 \cdot 10^8$ Vm^{-1}.

Let us use the coordinate system defined in Section 2.2.1. Assuming the direction of the particles to be parallel to the direction of the nominal particle beam, $\mathbf{v} = (0, 0, v_s)$, and the magnetic field to be of the form $\mathbf{B} = (B_x, B_z, 0)$ there will be a balance between the Lorentz force $F_x = -ev_sB_z$ and the centrifugal force $F_r = mv_s^2/R$. Where m is the relativistic particle mass. From this we get:

$$\frac{1}{R(x, z, s)} = \frac{e}{p} B_z(x, z, s) \qquad (2.5)$$

where $p = mv_s$.

Expanding the magnetic field in the close vicinity of the nominal path (the s-axis) results in[3]:

$$B_z(x) = B_{z0} + \frac{dB_z}{dx}x + \frac{1}{2!}\frac{d^2B_z}{dx^2}x^2 + \frac{1}{3!}\frac{d^3B_z}{dx^3} + ... \qquad (2.6)$$

for a set value of z.

Multiplying by e/p gives:

$$\begin{aligned}\frac{e}{p}B_z(x) &= \frac{e}{p}B_{z0} + \frac{e}{p}\frac{dB_z}{dx}x + \frac{e}{p}\frac{1}{2!}\frac{d^2B_z}{dx^2}x^2 + \frac{e}{p}\frac{1}{3!}\frac{d^3B_z}{dx^3} + ... \\ \frac{e}{p}B_z(x) &= \frac{1}{R} + kx + \frac{1}{2!}mx^2 + \frac{1}{3!}ox^3 + ...\end{aligned} \tag{2.7}$$

The right-hand side terms correspond to dipole, quadrupole, sextupole, and octupole fields, in that order[3]. These field orders correspond to different types of magnets in an accelerating structure, and each of them have unique effects on the particle beam.

2.2.3 Linear Beam Optics

In order to simplify calculations it is useful to consider the motion close to the nominal trajectory of the particle. This is a fair approach since the transverse beam size in a storage ring is small compared to the radius of the orbit. From this one can choose to represent the particle trajectory as a displacement, x_0, and a gradient, x_0', from the nominal orbit [3]. More simply put, x_0 is the displacement, and x_0' is the displacement angle. Corresponding terms also exist in the z-plane.

Using also the coordinate system defined in Section 2.2.1 the equations of motion for a particle moving through a linear lattice can be derived[3]:

$$\begin{gathered}x''(s) + \Big(\frac{1}{R^2(s)} - k(s)\Big)x(s) = \frac{1}{R(s)}\frac{\Delta p}{p} \\ z''(s) + k(s)z(s) = 0\end{gathered} \tag{2.8}$$

where $k(s)$ is strength of the quadrupole field (see Equation 2.7), and $\Delta p/p$ is the deviation in momentum from the value defined by the nominal path. Higher order terms are not present since the lattice is linear.

Using linear beam optics and the assumption that $R(s)$ and $k(s)$ are piece-wise constant the dipole, quadrupole fields, and drift sections can now be described as matrices[3]:

$$M_{dipole} = \begin{pmatrix} \cos\frac{s}{R} & R\sin\frac{s}{R} \\ -\frac{1}{R}\sin\frac{s}{R} & \cos\frac{s}{R} \end{pmatrix} \tag{2.9}$$

$$M_{quadrupole} = \begin{cases} \begin{pmatrix} \cos\Omega & \frac{1}{\sqrt{|k|}}\sin\Omega \\ -\sqrt{|k|}\sin\Omega & \cos\Omega \end{pmatrix} & \text{, if } k < 0 \\ \begin{pmatrix} \cosh\Omega & \frac{1}{\sqrt{k}}\sinh\Omega \\ \sqrt{k}\sinh\Omega & \cosh\Omega \end{pmatrix} & \text{, if } k > 0 \end{cases} \tag{2.10}$$

$$M_{drift} = \begin{pmatrix} 1 & s \\ 0 & 1 \end{pmatrix} \tag{2.11}$$

where $\Omega = \sqrt{|k|}s$.

The effect on the displacement and gradient is simply given by $\mathbf{MX}_0$ where $\mathbf{M}$ is the matrix representation of the optical element, a *transfer matrix*, and $\mathbf{X}_0 = [x_0\ x_0']^T$ is the initial displacement and gradient of a single particle. Additionally, as every optical element in a structure of linear magnetic elements can be represented by such a matrix, the effect of the entire lattice on the particles can be written as the multiplication of the individual elements.[3]

2.2.4 Beta Function

Using the equation of motion for particles in a focusing magnet lattice (Equation (2.8)) under the assumption that all particles have the nominal energy ($\Delta p = 0$) and that there are no dipole fields ($\frac{1}{R} = 0$) we get:

$$x''(s) - k(s)x(s) = 0 \tag{2.12}$$

This is a version of Hill's differential equation of motion with known solutions of the form[3]:

$$x(s) = Au(s)\cos[\Psi(s) + \phi] \tag{2.13}$$

The beta function, $\beta(s)$, can now be defined as:

$$\beta(s) \equiv u^2(s) \tag{2.14}$$

Equation (2.13) can now be written as[3]:

$$x(s) = \sqrt{\epsilon}\sqrt{\beta(s)}\cos[\Psi(s) + \phi] \tag{2.15}$$

where ϵ is known as the *emittance* of a single particle and is a constant of motion. Additionally, the *phase advance function*, Ψ, needs to satisfy the relation[3]:

$$\Psi(s) = \int_0^s \frac{\mathrm{d}\sigma}{\beta(\sigma)} \tag{2.16}$$

The derivative of Equation 2.15 with respect to s gives us:

$$x'(s) = -\sqrt{\frac{\epsilon}{\beta(s)}}\Big(-\frac{\beta'(s)}{2}\cos[\Psi(s) + \phi] + \sin[\Psi(s) + \phi]\Big) \tag{2.17}$$

Equation (2.15) and (2.17) describes the motion of a single particle. A beam of many particles, each with a random initial phase, ϕ, will have a beam size and divergence limited by the beta function and the beam emittance. The new beam emittance represents a statistical value depending on several different physical effects (such as emission of synchrotron radiation, intra beam scattering etc.). It can be shown that[3]:

$$\begin{aligned}
\sigma_{x,z}(s) &= \sqrt{\epsilon_{x,z}\beta_{x,z}(s)} \\
\sigma'_{x,z}(s) &= \sqrt{\epsilon_{x,z}\gamma_{x,z}(s)} \\
\gamma_{x,z}(s) &= \frac{1 + (\beta'_{x,z}(s)/2)^2}{\beta_{x,z}(s)}
\end{aligned} \tag{2.18}$$

where σ is the rms transverse beam size, σ' is the rms transverse beam divergence, and the subscripts x and z represent the horizontal and vertical transverse dimensions. These are in turn directly connected to the *flux*, F, *brightness*, S, and *brilliance*, B, of the circular accelerator[3]:

$$\begin{aligned} F &= \frac{\text{photons}}{\text{s } 0.1\%\text{BW A}} \\ S &= \frac{F}{2\pi\sigma'_x\sigma'_z} \\ B &= \frac{F}{4\pi^2\sigma_x\sigma_z\sigma'_x\sigma'_z} \end{aligned} \tag{2.19}$$

where the flux is defined as the number of photons per second emitted in an energy range corresponding to 0.1% of the energy band width, at a beam current of 1 A.

A lattice which has the possibility of generating high intensity light has a small electron beam emittance and beta function amplitude at the longitudinal positions of the insertion devices. Therefore the beta function directly corresponds to the performance of the *beam lines*, where experiments are run using the generated light, present at the machine.

The lattice has a net focusing effect, and within it the particles perform betatron oscillations. The *envelope function* is defined as[3]:

$$E(s) \equiv \sqrt{\epsilon\beta(s)} \tag{2.20}$$

Statistically 68.2 % of the particle trajectories lie within this envelope.

2.2.5 Dispersion

Assume instead that we have off-momentum particles ($\Delta p \neq 0$) moving through a magnetic structure without quadrupole fields ($k = 0$). Equation (2.8) now becomes:

$$x''(s) + \frac{1}{R^2(s)}x(s) = \frac{1}{R(s)}\frac{\Delta p}{p} \tag{2.21}$$

Using $\Delta p/p = 1$ we call the solution to this function the dispersion function, $x(s) = D(s)$, the general form of this solution and its derivative are[3]:

$$\begin{aligned} D(s) &= D_0 \cos\frac{s}{R} + D'_0 R \sin\frac{s}{R} + R\Big(1 - \cos\frac{s}{R}\Big) \\ D'(s) &= -\frac{D_0}{R}\sin\frac{s}{R} + D'_0\cos\frac{s}{R} + \sin\frac{s}{R} \end{aligned} \tag{2.22}$$

where $D_0 = D(0)$ and $D'_0 = D'(0)$.

The position of an off-momentum particle can now be written as the sum of the general and partial solution to Equation (2.8):

$$x_{\Delta p/p}(s) = x(s) + x_D(s) = x(s) + D(s)\frac{\Delta p}{p} \tag{2.23}$$

Here $x(s)$ is the transverse position of a particle with nominal momentum, and $x_D(s)$ is the transverse displacement due to the momentum of the particle.

Since the dispersion affects the beam size, synchrotron radiation sources are usually designed with zero dispersion at the points of the insertion devices.

2.2.6 Betatron Tune

The transverse motion of a particle travelling in a storage ring (see Equation 2.15) is oscillatory. The number of periods the particles are able to preform horizontally and vertically during one turn of the storage ring are known as the horizontal and vertical tunes. These are often referred to by their integer and fractional part.

From Equation (2.15) we get an expression for the horizontal tune:

$$\nu_x = \big(\Psi(L) - \Psi(0)\big)/2\pi \tag{2.24}$$

where L is the circumference of the machine. A corresponding expression exists in the vertical plane.

A storage ring also has a longitudinal tune, which the number of longitudinal oscillations performed during one turn of the ring. As this number is commonly much smaller than 1, the longitudinal tune is usually given in hertz.

2.2.7 Response Matrices

A way to characterise how changes in the lattice affect its properties is through *response matrices*. There are several different response matrices for a single lattice. Two of these, which are important for this thesis, are the linear response matrix and the orbit response matrix. These contain information on how properties of the lattice depend on the quadrupole gradients and on how the position of the beam depends on the strength of the dipole corrector magnets, respectively. A more in depth description can be found in Appendix A.

2.3 Magnets

Magnets in an accelerating structure or a storage ring are generally designed to generate a specific magnet multipole field; namely dipole, quadrupole, sextupole, octupole etc. These have different effects on the beam, a dipole field steers the beam, quadrupole focuses the beam, sextupole affects chromaticity (which will not be covered in this thesis) etc.

As the region close to the beam is vacuum it can be considered charge free. Thus, the potential function $V(x, z, s)$, which must be a solution to the charge free Laplace equation:

$$\Delta V \equiv 0 \tag{2.25}$$

can be used to derive the fields encountered by the electrons[2]. From a Taylor series expansion of the general solution the fields of the most commonly used magnets can be found[2]:

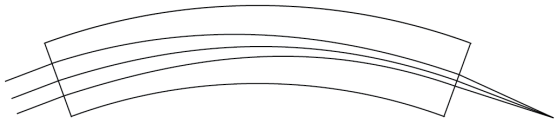

Figure 2.2: Edge focusing in a sector magnet dipole.

$$\begin{array}{ll} \text{Dipole} & -\frac{e}{p}V_1(x,z) = -\kappa_z x + \kappa_x z \\ \text{Quadrupole} & -\frac{e}{p}V_2(x,z) = -\frac{1}{2}\underline{k}(x^2 - z^2) + kxz \\ \text{Sextupole} & -\frac{e}{p}V_3(x,z) = -\frac{1}{6}\underline{m}(x^3 - 3xz^2) + \frac{1}{6}m(3x^2 z - z^3) \end{array} \tag{2.26}$$

where κ_z, κ_x, $\underline{k}$, k, $\underline{m}$ and m represent the strength of each multipole component. k and m represent the traditional magnet orientation, while $\underline{k}$ and $\underline{m}$ represent a pole structure rotated 45° around the s-axis.

Using the relation $\mathbf{B} = -\boldsymbol{\nabla}V(x,z)$[2] the corresponding magnetic fields of traditionally oriented magnets can be found:

$$\begin{array}{lll} \text{Dipole} & \frac{e}{p}B_x = 0 & B_z = \kappa_x \\ \text{Quadrupole} & \frac{e}{p}B_x = kz & \frac{e}{p}B_z = kx \\ \text{Sextupole} & \frac{e}{p}B_x = mxz & \frac{e}{p}B_z = \frac{1}{2}m(x^2 - y^2) \end{array} \tag{2.27}$$

As only dipoles, quadrupoles, and sextupoles are present in the MAX IV 1.5 GeV storage ring only these will be discussed below.

2.3.1 Types of Magnets

Dipole Magnets

Dipole magnets in a storage ring are used to steer the path of the particles. The nominal path is defined by the dipole fields. The magnetic field of a bending dipole is $B_z = \frac{\kappa_x}{(e/p)}$, with the relation $\kappa_x = 1/R$.

The total deflection angle of a dipole is given by:

$$\theta = \int \frac{1}{R}\mathrm{d}s = \int \frac{e}{p}B_{z0}\mathrm{d}s \tag{2.28}$$

A phenomenon known as *edge focusing* occurs in sector magnet dipoles, i.e. circle sector shaped dipoles, where particles enter and exit the magnet at the same longitudinal coordinate regardless of the transverse coordinate. Because of this particles with a positive horizontal displacement will travel further in the dipole and are thus bent more than particles on the nominal orbit. Particles with a negative horizontal displacement travel a shorter distance in the dipole and are bent less. This results in a sector dipole magnet having a net focusing effect (see Figure 2.2).[3]

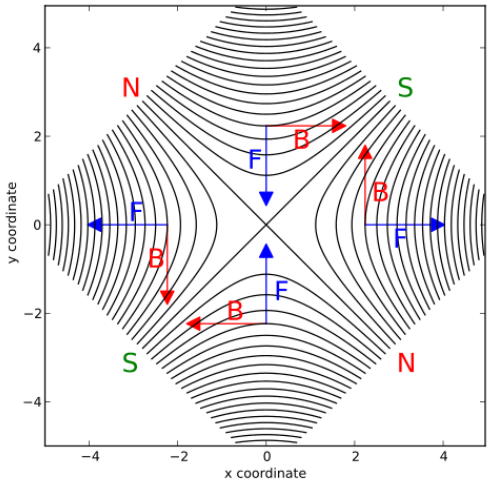

Figure 2.3: Idealised magnetic field of a quadrupole, with forces.[4]

Quadrupole Magnets

A pure quadrupole magnet consists of four magnetic poles of alternating polarity. When the poles are oriented 45° in relation to the horizontal and vertical transverse axes the quadrupole is always focusing in one plane and defocusing in the other (see Figure 2.3). In order to focus the beam in both planes it is necessary to have at least two quadrupoles in the lattice with opposite polarities. When placing the poles in the vertical and horizontal plane we will get coupling between the two planes. These *skew* terms correspond to the underlined quantities in Equation (2.26).

Sextupole Magnets

The sextupole magnets in a storage ring are used to correct for chromatic aberrations. Chromaticity is essentially the change in betatron tune due to particle energy deviation[3]:

$$\xi \equiv \frac{\Delta Q}{\Delta p/p} = \frac{1}{4\pi} \oint k(s)\beta(s)\mathrm{d}s \tag{2.29}$$

As the name suggests, and in analogy with the previously mentioned magnet types, the sextupole consists of six magnetic poles of alternating polarity.

Particles travelling through a sextupole at an off nominal transverse position will experience a quadruple field or a skew quadrupole field depending on the orientation of the poles. As previously mentioned a skew quadrupole field gives rise to coupling between the two transverse planes of the beam. This means that

an effect on the horizontal motion of the beam, for instance a horizontal dipole kick, will affect also the vertical beam motion, and vice-versa.[3]

2.3.2 Magnet Hysteresis

Magnet hysteresis is the concept that the history of the magnetisation of the electromagnet iron yoke affects the magnetic field produced by the magnet at a given current[5]. By establishing a known and reproducible magnet history it is possible for the magnet to enter a known hysteresis curve. From such a point changes in the current following the hysteresis curve give a known magnetic field strength. Any deviation from the curve will yield an unknown magnetic field strength.

2.4 RF Cavities

The energy lost by the electrons with each revolution in a storage ring, for instance the energy lost due to synchrotron radiation, must be replenished. This is achieved through RF cavities. The cavities contain electromagnetic fields, the electric component of which accelerates the passing particles. This field is a time harmonic standing wave with an amplitude varying in time which will accelerate the particles reaching the cavity when the field amplitude corresponds to a positive force in the direction of longitudinal motion, i.e. a negative electric field when accelerating negatively charged particles and a positive when accelerating positively charged particles. Thus a particle beam is not a continuous stream of particles but rather a *train* of particle *bunches*.

The maximum number of bunches which can be contained in a storage ring, a number referred to as *buckets*, can be calculated through:

$$\frac{L}{\beta c} f_{\mathrm{RF}} = n_{\mathrm{buckets}} \tag{2.30}$$

where L is the nominal path length of the beam, c is the speed of light, β is the fraction v/c (not to be confused with the beta function) where v is the speed of the particles, and f_{RF} is the frequency of the field in the cavities.

The momentum of the stored particles in a storage ring can be altered by decreasing or increasing the frequency in the cavities. A decrease in frequency corresponds to an increase in momentum. This is because a relativistic particle of higher momentum has its path bent less by the dipole bending magnets, thus it takes a path with a larger circumference around the ring. A longer path corresponds to it arriving less frequently at the accelerating cavity, which in turn corresponds to a lower frequency.[2]

The relation between the relative change in path length and the relative change in momentum is called the *momentum compaction factor*. It is defined as[3]:

$$\alpha = \frac{\Delta L/L}{\Delta p/p} \tag{2.31}$$

The change in path length due to the off-momentum of the particle, ΔL, is given by[3]:

$$\Delta L = \frac{\Delta p}{p} \oint \frac{D(s)}{R(s)} \mathrm{d}s \tag{2.32}$$

Using Equation (2.31) and (2.32) the momentum compaction factor can now be written as:

$$\alpha = \frac{1}{L_0} \oint \frac{D(s)}{R(s)} \mathrm{d}s \tag{2.33}$$

Chapter 3
MAX IV Storage Rings

The MAX IV laboratory consists of a linear accelerator (linac) which feeds two storage rings of different size, and a short pulse facility at the very end of the linac.

This report will mainly cover the smaller of the two storage rings.

3.1 The 1.5 GeV Storage Ring

The MAX IV 1.5 GeV storage ring is the smaller of the two storage rings present at the MAX IV facility. It has the same electron energy as the MAX II storage ring which was, until recently, still in operation. As there was, and is, interest from users to run experiments at beam lines using soft X-rays it was decided to build not only a large 3 GeV storage ring, but also a second smaller ring.

3.1.1 Magnet Structure

The 1.5 GeV storage ring lattice consists of 12 main magnet cells[6]. These are referred to as *achromats* since the exit positions are independent of the particle energies. As the path of the particles must be bent 360° in order to have a full orbit each achromat deflects the path by 30°. As the achromats are of the type Double Bend Achromat, or DBA, they contain two separate dipole bending magnets each with a bending angle of 15°[6]. Each achromat consists of a half-achromat joined up with an identical but mirrored half-achromat (see Figure 3.1). The mirrored symmetry is only broken by diagnostic devices, *BPM*s, and dipole corrector magnets[6], both of which are covered in this report.

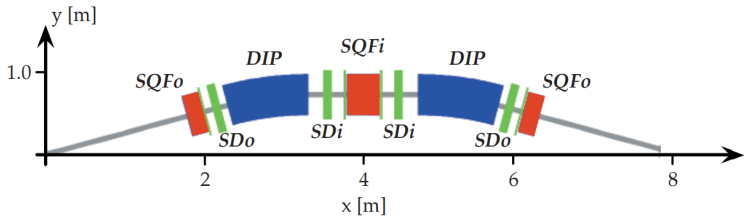

Figure 3.1: Schematic of a DBA of the 1.5 GeV storage ring.[6]

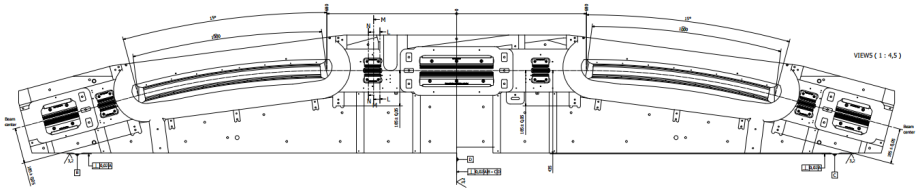

Figure 3.2: The 1.5 GeV storage ring machined magnet block.[7]

Each achromat consists of the magnets[6]:

- SQFO - The combined outer focusing quadrupole/sextupole
- SCO - The outer sextupole corrector
- SDO - The outer defocusing sextupole
- DIP - Dipole 15° bending magnet
- SDI - The inner defocusing sextupole
- SCI - The inner sextupole corrector
- SQFI - The combined inner focusing quadrupole/sextupole

A magnet referred to as focusing is in this case focusing in the horizontal plane unless otherwise stated. Note that the achromat is lacking defocusing (vertically focusing) quadrupoles. The vertical focusing can instead be found in the bending dipole magnets, which due to their shape contain both dipole and quadrupole fields. These are fitted with *Pole-Face Strips* to allow for tunability of the defocusing quadrupole component.[8]

Each achromat also contains six dipole correctors, half in the horizontal plane, and half in the vertical plane. These do not have separate iron yokes but are instead extra windings on the already existing sextupoles. Specifically on the SCO magnets and the second SCI in each achromat. These extra windings are also used as skew quadrupoles, which can be used to compensate for coupling in the machine.[8]

The achromats of both the MAX IV 1.5 GeV ring and 3 GeV ring (which is not covered here) have several magnets with a shared iron yoke. In the 1.5 GeV storage ring all magnets in each achromat are milled out of the same iron block (see Figure 3.2). The conventional magnet design is to have one yoke per magnet, which are aligned individually. Having several magnets in the same iron block is both inexpensive and reduces the number of elements to align, as the magnets in each block are already aligned within the error of machining accuracy (order of 10 µm)[9].

Each magnet family (family referring to SQFO, DIP etc.) in the ring have a common power supply, to which the magnets are connected in series. This approach is more cost effective, and results in the same current in all magnet coils belonging to magnets of the same family. As some measurements, for instance BPM offset measurements, require the ability to alter the focusing gradient of

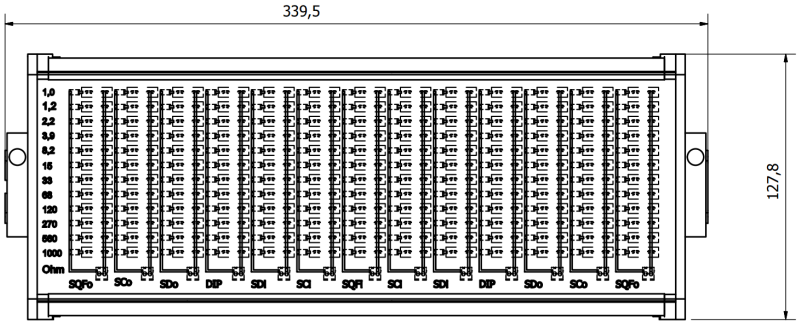

Figure 3.3: Schematic of the shunt resistance circuit of the 1.5 GeV storage ring. Measurements are in mm.[10]

a single magnet all three quadrupoles in each achromat are fitted with a relay controlled shunt resistance. When active the shunt reduces the current through its magnet by a small fraction.

In addition to the relay controlled shunts each magnet block is fitted with a shunt resistance circuit board (see Figure 3.3). As there is only one power supply per magnet family, static individual magnet field errors (difference in strength) are meant to be corrected using these shunts. By connecting the shunts in parallel to the magnet coils each magnet can be given an individual current value resulting in a magnet strength close to the nominal.

3.2 Diagnostics

3.2.1 Beam Position

One of the most important monitoring devices in an accelerator is the beam position monitor, or BPM. As the name suggests the BPM can detect the transverse position of the electron beam at a given longitudinal position. More specifically it detects the charge centre of the beam.

The 1.5 GeV storage ring BPMs consist of four electrodes arranged symmetrically around the beam axis at the same longitudinal position. As the 1.5 GeV storage ring vacuum chamber is wider horizontally the electrodes are placed at an angle of 37.5° and 90° in respect to the horizontal axis (see Figure 3.4). This brings the electrodes closer to the beam which gives a more accurate reading. The arrangement also minimises the risk of synchrotron radiation from the dipoles or insertion devices hitting the electrodes. Radiation could produce systematic errors (due to the photo-electric effect or heating), or damage the electrode. The BPMs in the centre of each magnet block have a different electrode placement compared to the BPms at the end of the blocks (see Figure 3.4). This is simply because the BPM cabling would not fit if the in the middle of the magnet blocks if the angled electrode placement was used.

The signal of an electrode is the result of the displacement current occurring

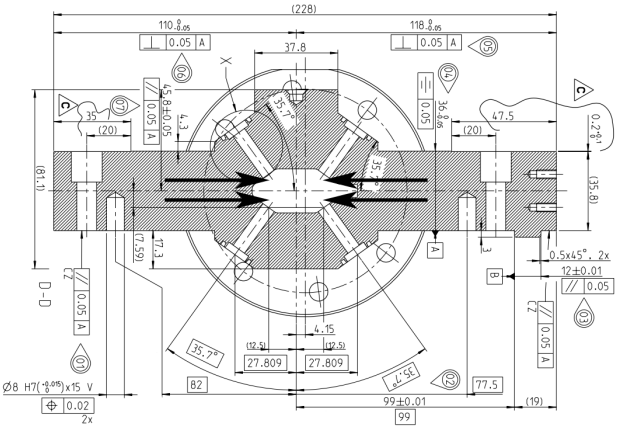

(a) The design of the 1.5 GeV storage ring BPMs located at the ends of each magnet block. Electrode heads have been marked with arrows.[11]

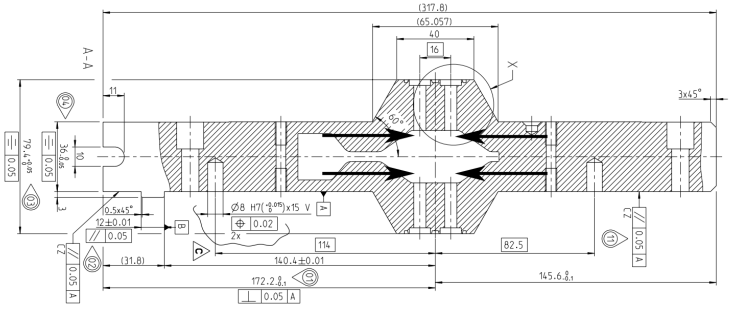

(b) The design of the 1.5 GeV storage ring BPMs located in the middle of each magnet block. Electrode heads have been marked with arrows.[12]

Figure 3.4: The two BPM designs used in the 1.5 GeV storage ring.

when the relativistic electron bunch passes the BPM. The intensity of the signal depends on the distance to the charge centre of the beam. Although the intensity function is relatively complicated $\mathbf{I}_{\text{intensity}} \propto 1/\mathbf{r}$ is a good approximation, where $\mathbf{r}$ is the distance from the charge centre of the beam to the electrode[3]. With the signal of all four electrodes it is possible to determine the transverse displacement of the charge centre of the beam[3]:

$$\begin{aligned} \Delta x &= a\frac{(I_2 + I_3) - (I_1 + I_4)}{\sum_{j=1}^{4} I_j} \\ \Delta z &= a\frac{(I_1 + I_2) - (I_3 + I_4)}{\sum_{j=1}^{4} I_j} \end{aligned} \tag{3.1}$$

The constant a, BPM *gain*, is determined theoretically from the shape of the BPM

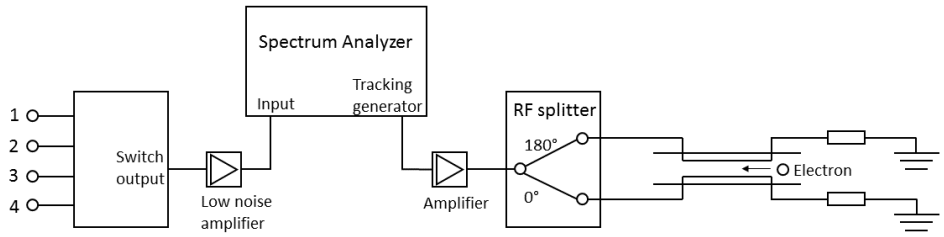

Figure 3.5: Block diagram of the tune measurement.

electrode heads.

Ideally a beam in the centre of the BPM will result in all four signals having the same intensity. However due to imperfections of the electrodes, the shape of the vacuum chamber, the cabling and the electronics this is rarely the case. If the BPM reports a stable value it is possible to measure the *offset* of the BPM. This is done by finding the centre of a nearby quadrupole using the electron beam, which is then taken as the zero value of the BPM. Machining precision on the magnet blocks are in the order of 10 µm from the nominal beam path[9]. This is more accurate than electrically calibrating the BPMs which due to previously mentioned factors commonly has an accuracy of $100 - 300$ µm.

3.2.2 Tune

The tune measurement setup at the MAX IV storage rings consists of a spectrum analyser connected to a BPM and a strip-line inside of the vacuum chamber of the ring. The output signal of the spectrum analyser sweeps over an adjustable frequency span. The signal is amplified before reaching the strip-line which is able to excite the beam, either horizontally, vertically, or diagonally, with the frequency provided by the spectrum analyser. The signal from the BPM is also amplified before reaching the spectrum analyser (see Figure 3.5). If the excitation frequency matches that of the betatron tune the beam will be excited and give a higher response in the BPM. A phenomena known as SR dampening keeps the beam from becoming unstable, despite exciting it at a resonant frequency. The spectrum analyser also shows peaks at the harmonics of the revolution frequency. These peaks are used as reference points when measuring the tune (see Figure 3.6). Below follows a simple derivation as to how the peaks on a spectrum analyser occurs.

The signal of the BPM is proportional to the charge distribution, f. It receives a signal for every turn performed in the machine:

$$I(t) \propto \sum_{n}^{\infty} f(t - nT) \tag{3.2}$$

where n is the turn number, and T is the revolution period of the machine.

The signal is also proportional to the horizontal and vertical position of the electron bunch, depending on which tune is measured:

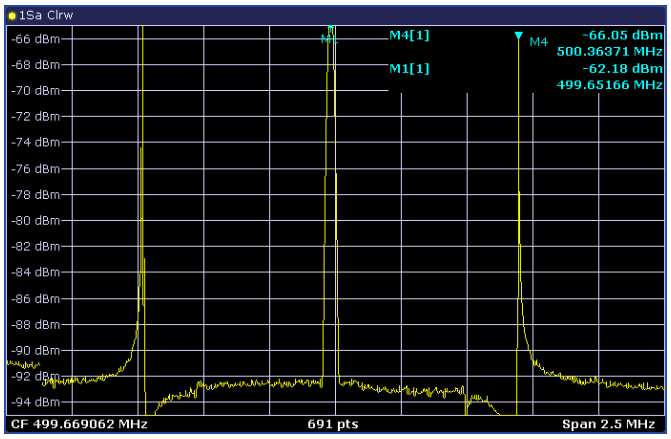

Figure 3.6: Spectrum analyser window. Centre peak is the revolution frequency, and the two sidebands are the horizontal tune resonances.

$$I \propto \Delta x_\beta \tag{3.3}$$

which in turn is proportional to the betatron oscillations which have the frequency ω_β:

$$\Delta x_\beta \propto \cos(\omega_\beta t) \propto e^{j\omega_\beta t} + e^{-j\omega_\beta t} \tag{3.4}$$

The signal intensity becomes:

$$I \propto \sum_n^\infty f(t - nT)(e^{j\omega_\beta t} + e^{-j\omega_\beta t}) \tag{3.5}$$

The Fourier transform of Equation (3.2) results in the revolution peaks on the spectrum analyser. Each element in the sum becomes:

$$\mathscr{F}(I_n) \propto \mathscr{F}(f(t - nT)) = F_n(\omega) \tag{3.6}$$

while the Fourier transform of Equation (3.5) results in the tune side-bands:

$$\mathscr{F}(I_n) \propto \mathscr{F}(f(t - nT)(e^{j\omega_\beta t} + e^{-j\omega_\beta t})) = F_n(\omega + \omega_\beta) + F_n(\omega - \omega_\beta) \tag{3.7}$$

Hence, the betatron frequency can be measured as the frequency spacing between the tune peak and its corresponding revolutionary frequency. The tune is calculated as:

$$\nu_x = \frac{\omega_\beta}{\omega_{\text{rev}}} \tag{3.8}$$

Note that it is only possible to measure the fractional tune with this measurement. However, the integer of the tune is easily found by applying a dipole kick to

the beam and looking at the betatron oscillations which occur (see Equation 8.4). This method requires there to be at least twice as many BPMs as the number of oscillations performed.

3.3 Software

The MAX IV Laboratory uses Matlab for most of its simulations of and communications with the storage rings. The Matlab language was chosen due to already existing libraries for both the simulations, communication, control and calibration routines (Accelerator Toolbox and Matlab Middle Layer). These have already been used at a large number of other facilities around the world.

3.3.1 Matlab Middle Layer

Communications with either the simulator or with the hardware (via a TANGO integration layer) is done through the *Matlab Middle Layer*, or MML[8].

MML is a Matlab library containing functions which can communicate with the simulator and the hardware. Originally a part of the ALS's (Advanced Light Source) and the SSRL's (Stanford Synchrotron Radiation Lightsource) control system, the MML was made machine independent and is now easily ported to other machines[13].

3.3.2 TANGO

TANGO Controls is a free open-source object oriented software toolkit[14]. All communications from Matlab and MML to the hardware goes through the TANGO system.

3.3.3 Accelerator Toolbox

The MAX IV facility uses the Matlab toolbox *Accelerator Toolbox*, or AT, for its simulations of the storage rings. It was originally developed for the SPEAR3 light source, but has since then been used at many other facilities[15]. The AT contains a collection of tools for manipulating accelerator data structures, simulate particle motion, and calculate beam properties and accelerator parameters.

3.3.4 Linear Optics from Closed Orbits

Linear Optics from Closed Orbits, or LOCO, is an algorithm which can be used for debugging the optics of a storage ring[16]. It uses a measured orbit response matrix of the ring which it fits to a model response matrix. From this a model which best reproduces the measured orbit response matrix can be produced[16].

The LOCO algorithm minimises the difference the measured and the model orbit response matrix[16]:

$$\chi^2 = \sum_{i,j} \frac{\mathbf{A}_{\mathrm{model},ij} - \mathbf{A}_{\mathrm{measured},ij}}{\sigma_i^2} \equiv \sum_{k=i,j} E_k^2 \tag{3.9}$$

where σ_i is the noise level of the i:th BPM.

The minimisation is achieved by iteratively solving[17]:

$$\begin{aligned} E_k^{i+1} &= E_k^i + \frac{\partial E_k^i}{\partial K_l} \Delta K_l = 0 \\ -E_k^i &= \frac{\partial E_k^i}{\partial K_l} \Delta K_l \end{aligned} \tag{3.10}$$

for ΔK_l. These are the changes in fit parameters which LOCO is configured to fit. The terms $\frac{\partial E_k^i}{\partial K_l}$ can be identified as elements of the linear response matrix (see Appendix A).

LOCO can be given many different parameters to fit. Common parameters are BPM gains, corrector magnet kicks, quadrupole fields, and BPM and corrector magnet coupling. But magnet positions and rotations can also be fitted. Additionally LOCO can also fit the model dispersion pattern to the dispersion of the machine. This is done by simply adding the dispersion pattern as an additional column in the orbit response matrix. The pattern is used by LOCO to determine the ratio between the dipole corrector kicks and the BPM gains. The model reported by LOCO can then be used to alter the storage ring so that its performance is closer to that of the model.

Like any other fitting, if LOCO is given more degrees of freedom than variables to fit to it can arrive at several different solutions. Thus it might be advantageous to run several LOCO fittings of the same data with different parameters to fit on each.

Chapter 4
Methodology

4.1 Procedure

For the measurements and analysis of the 1.5 GeV storage ring characteristics the following procedure was followed:

- BPM Offsets
  - The effect of magnet hysteresis on the BPM offset measurements was investigated
  - New modified BPM offset measurements techniques were implemented and evaluated
- LOCO
  - Methods were tested to measure the response matrix and dispersion with high reproducibility
  - LOCO fits with different parameter configurations were made to the measured data
- Tune-shift
  - Reproducibility of tune-shift measurements were tested
  - Beta-function at the quadrupoles was calculated

4.2 Measurement Methods

4.2.1 BPM Offsets

In order to be sure that the BPMs of the machine report displacements in relation to the the true nominal path of the particles it is necessary to calibrate the BPMs. This is done by measuring the offset of the value reported by the BPM. The measurement procedure used is often called *Beam Based Alignment*, or BBA.

When measuring the offsets the fact that the strength of the magnetic fields in the centre of the quadruples is zero is used. This also holds true for higher order magnets, but quadrupoles are used because they give rise to a first order effect on

a displaced beam (see Equation (2.27)). When the beam is perfectly centred in a quadrupole any change in field strength will give no beam response. The effect on an off-centre beam is linearly dependent on the strength of the quadrupole.

Offset measurements in the 1.5 GeV storage ring use the quadrupole magnet closest to the relevant BPM. These quadrupoles belong to the SQFI family in the case of the BPMs in the centre of the magnet block, and the SQFO family in the case of the BPMs in the beginning and end of the magnet block. Using a dipole corrector magnet the beam is placed at a few different positions in the BPM. These are either in the horizontal or vertical plane depending on which offset is to be measured. At each beam position the shunt of the quadrupole closest to the BPM is switched on and off.

The shunting of the quadrupole will result in an effect on the beam which is linear with respect to the displacement in that magnet (see Equation (2.27)). The difference in displacement reported by the BPMs with the shunt on or off can be linearly fitted against the beam placements in the BPM which is closest to the quadrupole. From this fit the BPM position which gives the smallest effect on the orbit when changing the quadrupole strength can be found. This position corresponds to the centre of the quadrupole, which is assumed also be the centre of the BPM (see Figure 4.1). Thus, the BPM readings of the yet calibrated BPM at this beam position corresponds to the horizontal and vertical offset values.

4.2.2 Orbit Response Matrix

The orbit response matrix of a storage ring and its model can be measured as[18]:

$$\begin{pmatrix} x \\ y \end{pmatrix} = A \begin{pmatrix} \theta_x \\ \theta_y \end{pmatrix} \tag{4.1}$$

where θ_x and θ_y are the changes in dipole corrector strengths, and x and y are the resulting perturbations of the electron beam orbit.

The current amplitude of the dipole kicks were chosen to be 10 % of the total current range of the corrector power supplies (1.15 A for the HCM and 1.05 A for the VCM). This amplitude gave a sufficient signal to noise ratio without causing any of the correctors to be saturated. Additionally half of the kick amplitude was applied negatively and half positively. For an ideal machine the response from the positive kick should be the inverse of the response from the negative kick (see Equation (8.4)). The orbit response is then calculated as:

$$A_{ij} = \frac{x_{j,\mathrm{pos}} - x_{j,\mathrm{neg}}}{\Delta\theta_{x,i}} \tag{4.2}$$

where A_{ij} is an element in the orbit response matrix, x_j is the horizontal read value of the j:th BPM, and $\Delta\theta_{x,i}$ is the dipole kick of the i:th horizontal corrector. The corresponding expression exists in the vertical plane.

As the orbit response matrix is to be used to correct linear optics it should ideally be measured in a lattice without sextupole fields, especially without sextupole magnets. However, it is not currently possible to have stored beam in the 1.5 GeV storage ring without sextupoles, since some sextupole fields are designed into the quadrupole magnets.

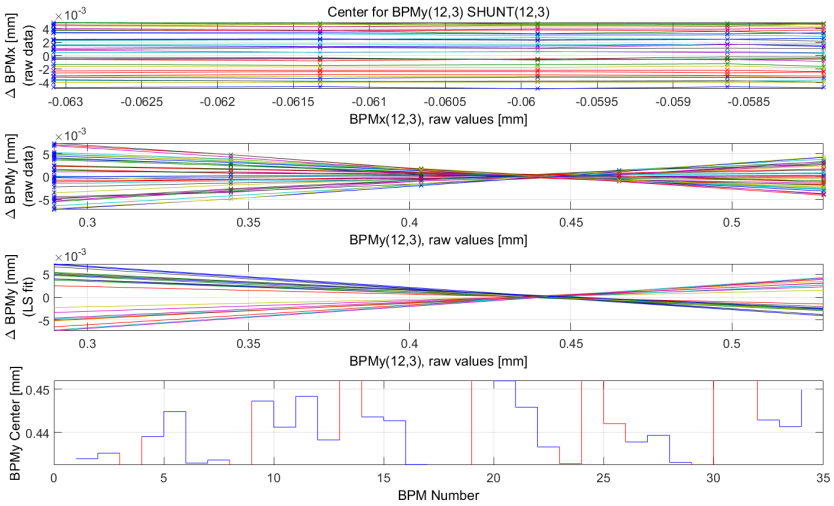

Figure 4.1: Linear fit of BPM response when measuring vertical offset in the last BPM achromat 12. Top: Difference in horizontal BPM readings before and after shunting plotted against the vertical BPM reading in the BPM to be measured. Second from top: Difference in vertical BPM readings before and after shunting plotted against the vertical BPM reading in the BPM to be measured. Second from bottom: Same data as second from top but fitted linearly. Fits with too small a gradient have been removed. Bottom: Vertical readings from BPMs corresponding to the zero crossing in the BPM to be measured.

4.2.3 Dispersion

The dispersion of the machine can easily be measured at each BPM. As seen in Equation (2.23), the dispersion is simply a displacement due to a unit relative momentum difference of the electrons. By increasing or decreasing the frequency of the accelerating RF the momentum of the particles can be altered. The dispersion at a BPM is then simply given by:

$$\begin{pmatrix} D_x(s_i) \\ D_y(s_i) \end{pmatrix} = \frac{1}{\Delta p/p} \begin{pmatrix} x_D(s_i) \\ y_D(s_i) \end{pmatrix} \tag{4.3}$$

where D_x and D_y are the horizontal and vertical dispersion, $\Delta p/p$ is the relative change in momentum due to the change in RF, and x_D and y_D is the dispersive transverse displacement (see Equation (2.23)).

The change in RF for the dispersion measurements was chosen to be 1500 Hz. The relative change in frequency is assumed to be inversely proportional to the relative change in electron path length. This is a good approximation for electrons of energy much higher than their rest energy as their speed is virtually constant. The relative change in momentum can then be calculated using Equation (2.31). As with the orbit response matrix half of the change in RF was applied positively, and half negatively.

4.2.4 Tune-Shift

The tune of a storage ring depends mainly on the quadrupole fields in the machine. For small changes in the quadrupole field of a magnet, Δk, we have[3]:

$$\Delta Q_{\mathrm{h,v}} = \frac{1}{4\pi} \int_{s_0}^{s_0+l} \Delta k \beta_{\mathrm{h,v}}(s) \mathrm{d}s \approx \frac{\Delta k}{4\pi} \langle \beta_{\mathrm{h,v}} \rangle l \tag{4.4}$$

where ΔQ is the change in tune, s_0 is the longitudinal position corresponding to the start of the magnet and l is the effective magnet length.

By intentionally changing the gradient of a single magnet by a known Δk and measure the shift in horizontal and vertical tune, it is possible to find the integrated average of the beta function inside the magnet:

$$\langle \beta_{\mathrm{h,v}} \rangle = \frac{\Delta Q_{\mathrm{h,v}}}{\Delta k} \frac{4\pi}{l} \tag{4.5}$$

The change of gradient was done with the relay controlled shunts on the quadrupole magnet (see Section 3.1.1). In order to find the size of the change in focusing gradient from having the shunt connected to the main coil of the magnet, the resistance of the shunt and the main coil was measured. The change in tune was measured using the spectrum analyser (see Section 3.2.2).

4.3 Magnet Hysteresis Compensation

4.3.1 Cycling

In order to establish a known and reproducible hysteresis curve in the magnets they are put through the procedure of *cycling*. Cycling consists of slowly bringing up the power supplies of the main coils of the magnets to their maximum setpoints in a number of controlled steps. After a small time plateau the power supplies are brought down to zero in the same manner. This is repeated for a number of iterations large enough for the magnet history prior to the cycling not to affect the field of the magnets.

All magnets in each achromat in the MAX IV 1.5 GeV storage ring are part of the same iron block. As this means that magnet yokes are connected the magnets of the ring are synchronously cycled. This is a way of compensating for cross-talk which is present between neighbouring magnets. Cross-talk refers to the magnetic field of one magnet leaking to another magnet in the same magnet block.

Extra windings on the magnet yokes are not cycled. As they share iron yoke with larger coils it has proven sufficient to only cycle the main coils of these magnets. For instance the dipole correctors HCM and VCM on the sextupoles SCO and SCI are not cycled, but the SCO and SCI coils are.

4.3.2 Dipole Corrector Magnets

As the dipole corrector magnets are used to correct the beam, often continuously, these are very rarely on their initial hysteresis curve. As long as the orbit of the beam is corrected to its initial position the magnetic field produced by the dipole corrector magnet is the same. Thus, the hysteresis of the dipole correctors does not need to be corrected for.

4.4 AT Lattice

The 1.5 GeV storage ring Accelerator Toolbox model lattice used for the simulations contains all magnet families present in the accelerator. The lattice consists of four different achromat structures, one of which is repeated nine times to make twelve achromats. The first and last achromat contains element related to the injection point, while the second contains the fast dipole kicker, or *pinger*.

In order to relate magnet current setpoint to magnetic fields the AT model has calibration curves for all magnet families. These are linear fits of manufacturer provided magnetic field data measured at different main coil currents. The maximum field order for the different calibration curves can be seen in Table 4.1. As each magnet family, except the dipole correctors (HCM and VCM), is connected in series with a single power supply the measured field data was averaged over all magnets in the family. This averaging was not done for the dipole correctors.

To better represent the longitudinal fringe field of the magnets, the dipole bending magnets and the quadrupoles in the model are represented by several smaller magnet slices in succession. The dipole are split up into 30 slices each,

Magnet Family	Field Order(s)
DIP	4
SQFI	2 to 3
SQFO	2 to 3
SCI	1 to 3
SCO	1 to 3
SDI	3
SDO	3
HCM	1
VCM	1
SCISKW	2
SCOSKW	2

Table 4.1: Maximum field order for AT model calibration curves.

while the quadrupole families SQFO and SQFI are split up into three and four slices respectively. The field distributions of these slices can be found in Appendix B.

The dipole corrector magnets are represented as thin (zero length) elements inside the SCO and SCI magnets.

Chapter 5
Measurement Results

5.1 BPM Offsets

As the offset measurements will be affected by hysteresis from two separate sources measurements were taken to assess the order of the hysteresis induced errors, and how effectively they can be corrected for. The two hysteresis sources are the relay controlled shunts causing the quadrupoles to enter a new unknown hysteresis curve, thus altering the optics, and the corrector hysteresis which somewhat shifts the closed orbit when resetting the current values of the correctors.

5.1.1 Uncorrected Measurements

The pre-existing method for determining the BPM offsets of the 1.5 GeV storage ring consists of:

1. Establishing a hysteresis loop in the quadrupole closest to the BPM which is to be measured. This is done by setting the shunt to on and off five times.
2. Placing the beam at five positions in the BPM. For each position the readings of all BPMs are recorded both with the shunt on and off.
3. Linearly fitting the difference in BPM reading with the shunt on and off against the position in the BPM to be measured.

This procedure is repeated for each separate BPM offsets to be measured. When measuring all the BPM offsets in the storage ring a hysteresis loop will have been established on all the quadrupoles. Thus, in order to find the reproducibility of the measurement the ring has to be cycled between each campaign.

Results from measurements using this method can be found in Figure 5.1.

The effect the change in optics has on the measured BPM offsets was investigated by measuring the offsets both in the direction achromat 1 to 12 as well as achromat 12 to 1. The difference can be seen in Figure 5.2.

5.1.2 Preemptively Established Hysteresis Loop

The BPM offset measurement procedure was altered to:

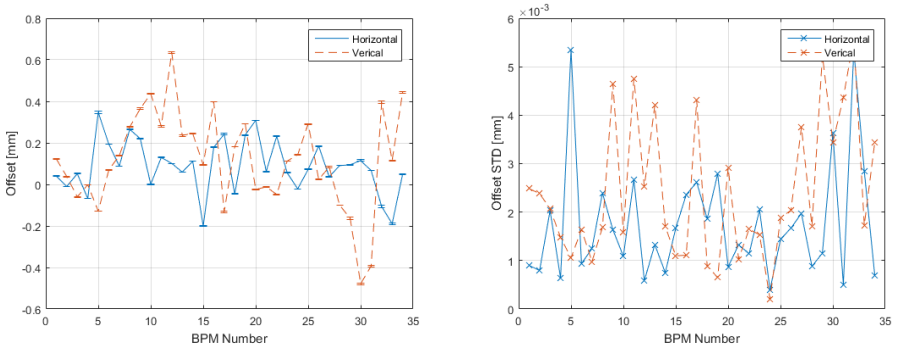

(a) Horizontal and vertical offsets measured using the standard (see Section 5.1.1) measurement procedure. The error bars represent 2σ of three measurements taken 2017-03-13 - 2017.03-19. The measurements were taken in the order achromat 1 through 12.

(b) Standard deviation, σ, of three horizontal and vertical offset measurements using the standard measurement procedure. The measurements were taken 2017-03-13 - 2017.03-19. The measurements were taken in the order achromat 1 through 12.

Figure 5.1: Measured BPM offsets using the default measurement method.

1. Establishing a hysteresis loop on all quadrupoles to be used during the measurement. This is done by setting the shunts to on and off ten times.

2. Correcting the orbit to sub-micron deviation in all BPMs for which this was possible (see Figure 5.13).

3. Placing the beam at five positions in the BPM. For each position the readings of all BPMs are recorded both with the shunt on and off.

4. Linearly fitting the difference in BPM reading with the shunt on and off against the position in the BPM to be measured.

Note that unlike the pre-existing procedure the hysteresis loop is established on all quadrupoles before the measurement continues. Point 3 and 4 are then repeated for each BPM offset to be measured.

The number of times the shunts had to be set on and off in order to establish a reproducable hysteresis loop was investigated using the tune-shift which arises from the change in quadrupole gradient (see Equation (4.4)). The resulting shift in tune for an arbitrarily chosen subset of shunted quadrupoles can be seen in Figure 5.3 and Table 5.1. Based on these results the shunts were set on and off for 10 iterations and the orbit was corrected to the previously measured offsets prior to starting the measurement.

The results of the offset measurements done on a machine with a preemptively established hysteresis loop can be seen in Figure 5.4.

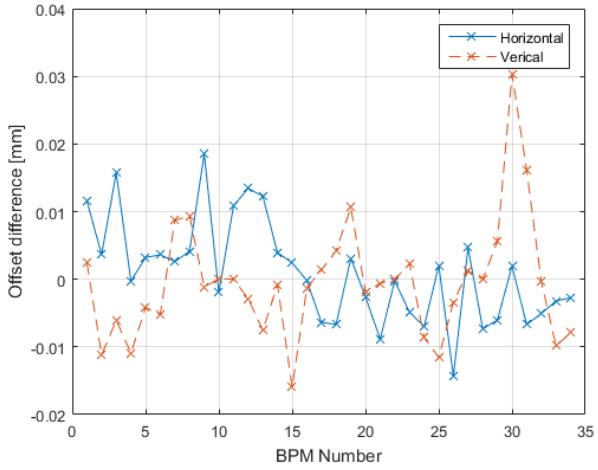

Figure 5.2: Difference in measured BPM offsets depending on the direction of measurement when using the default measurement method.

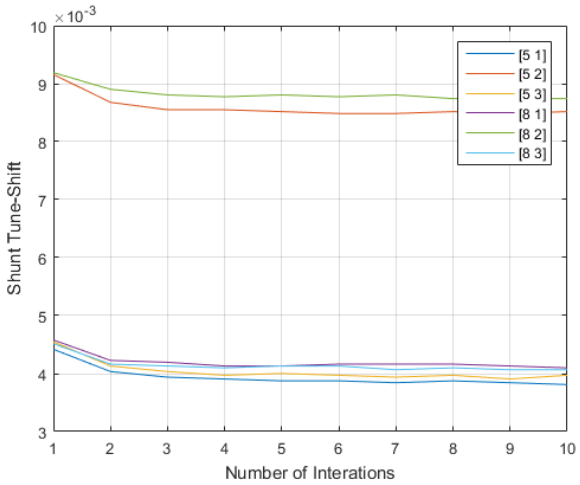

Figure 5.3: Observed tune-shifts when setting the shunts of the quadrupoles on and off for 10 iterations. The measurement was done using the quadrupoles in achromat 5 and 8.

Iteration	[5 1]	[5 2]	[5 3]	[8 1]	[8 2]	[8 3]
1	0.00442	0.00916	0.00455	0.00458	0.00919	0.00452
2	0.00403	0.00868	0.00413	0.00423	0.00890	0.00416
3	0.00394	0.00855	0.00403	0.00419	0.00881	0.00413
4	0.00391	0.00855	0.00397	0.00413	0.00877	0.00410
5	0.00387	0.00852	0.00400	0.00413	0.00881	0.00413
6	0.00387	0.00849	0.00397	0.00416	0.00877	0.00413
7	0.00384	0.00849	0.00394	0.00416	0.00881	0.00407
8	0.00387	0.00852	0.00397	0.00416	0.00874	0.00410
9	0.00387	0.00849	0.00391	0.00413	0.00874	0.00407
10	0.00381	0.00852	0.00397	0.00410	0.00874	0.00407

Table 5.1: Horizontal tune-shift when pulling quadrupole shunts (see Figure 5.3).

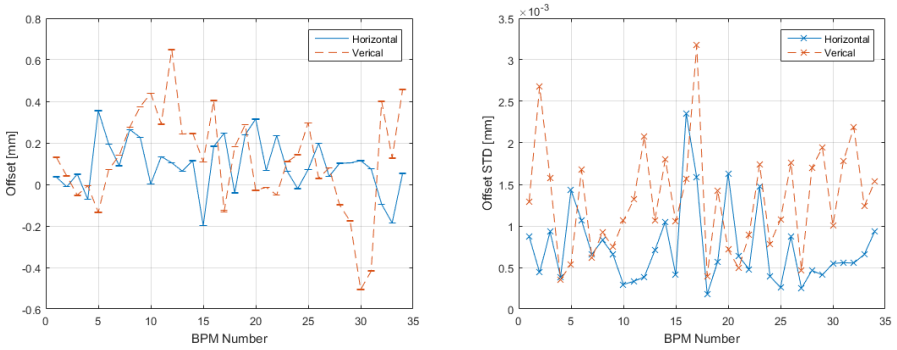

(a) Horizontal and vertical offsets measured after preemptively establishing a hysteresis loop (see Section 5.1.2). The error bars represent 2σ of five measurements taken 2017-03-15 - 2017.03-16. The measurements were taken in the order achromat 1 through 12.

(b) Standard deviation, σ, of five horizontal and vertical offset measurements after preemptively establishing a hysteresis loop. The measurements were taken 2017-03-15 - 2017.03-16. The measurements were taken in the order achromat 1 through 12.

Figure 5.4: Measured BPM offsets after preemptively establishing a hysteresis loop using the shunts.

Using this method the offsets were also measured in the direction achromat 1 to 12. The difference between measurements in different directions can be seen in Figure 5.5.

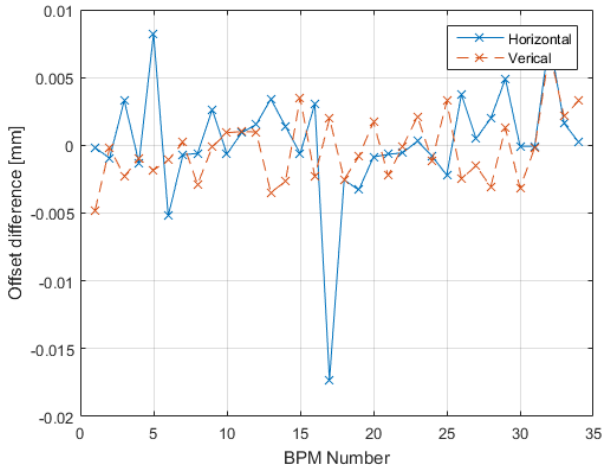

Figure 5.5: Difference in measured BPM offsets depending on the direction of measurement when measuring after preemptively establishing a hysteresis loop.

5.1.3 Corrected Orbit and Preemptively Established Hysteresis Loop

The measurement procedure was further modified to include orbit correction:

1. Establishing a hysteresis loop on all quadrupoles to be used during the measurement. This is done by setting the shunts to on and off ten times.
2. Correcting the orbit to sub-micron deviation in all BPMs for which this was possible (see Figure 5.13).
3. Placing the beam at five positions in the BPM. For each position the readings of all BPMs are recorded both with the shunt on and off.
4. Linearly fitting the difference in BPM reading with the shunt on and off against the position of the BPM to be measured.
5. Correcting the orbit to sub-micron deviation in all BPMs for which this was possible (see Figure 5.13).

Point 1 and 2 are done once at the beginning of the measurement, while the remaining points are done once per BPM offset to be measured.

As offset measurements with the quadrupoles on their original hysteresis curve are very time consuming (they require a full cycling of the ring, and reinjection) no measurements with correction without preemptively establishing a hysteresis loop were done.

The results of the measurements done with preemptively established hysteresis loops and orbit correction can be seen in Figure 5.6.

For the BPMs in which the vertical orbit could not be corrected a vertical reference orbit was set. The measurements with correction were redone with the

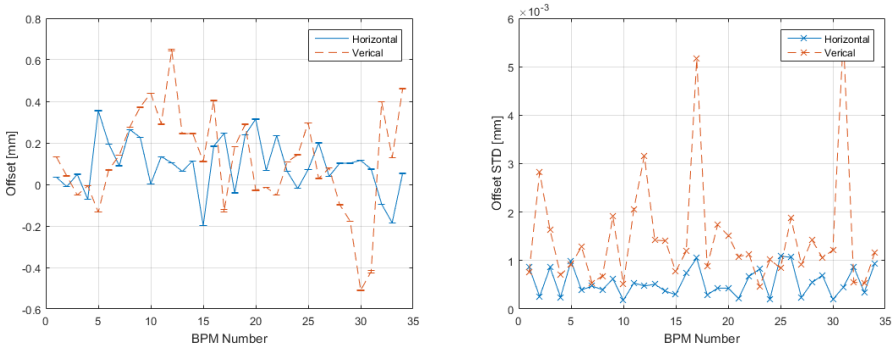

(a) Horizontal and vertical offsets measured with correction after preemptively established a hysteresis loop (see Section 5.1.3). The error bars represent 2σ of five measurements taken 2017-03-16 - 2017-03-17. The measurements were taken in the order achromat 1 through 12.

(b) Standard deviation, σ, of five horizontal and vertical offset measurements with correction after preemptively established a hysteresis loop. The measurements were taken 2017-03-16 - 2017-03-17. The measurements were taken in the order achromat 1 through 12.

Figure 5.6: Offsets measured with correction after preemptively established a hysteresis loop.

beam now being corrected vertically to this reference. This will ensure that the measurements are all done on the same orbit. The results from this measurement can be seen in Figure 5.7.

The difference in found BPM offset values when measuring in the direction achromat 1 through 12 compared to 12 through 1 can be seen in Figure 5.8.

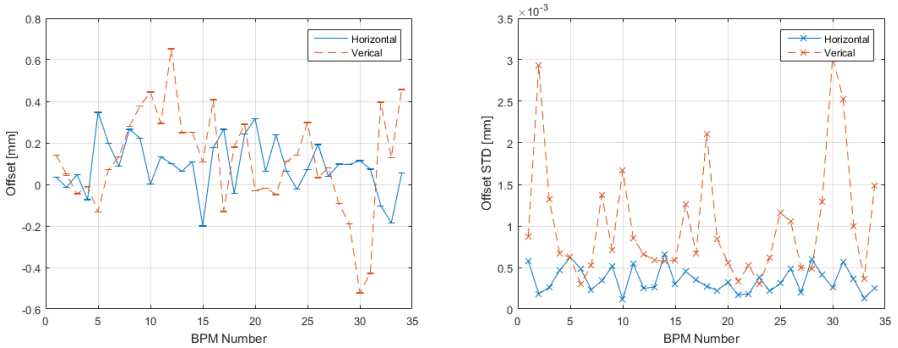

(a) Horizontal and vertical offsets with correction measured after preemptively established a hysteresis loop. Some BPMs were corrected to a non-zero offset. The error bars represent 2σ of five measurements taken 2017-04-01 - 2017-04-02. The measurements were taken in the order achromat 1 through 12.

(b) Standard deviation, σ, of five horizontal and vertical offset measurements with correction after preemptively established a hysteresis loop. Some BPMs were corrected to a non-zero offset. The measurements were taken 2017-04-01 - 2017-04-02. The measurements were taken in the order achromat 1 through 12.

Figure 5.7: Offsets measured when correcting some BPMs to a non-zero offset.

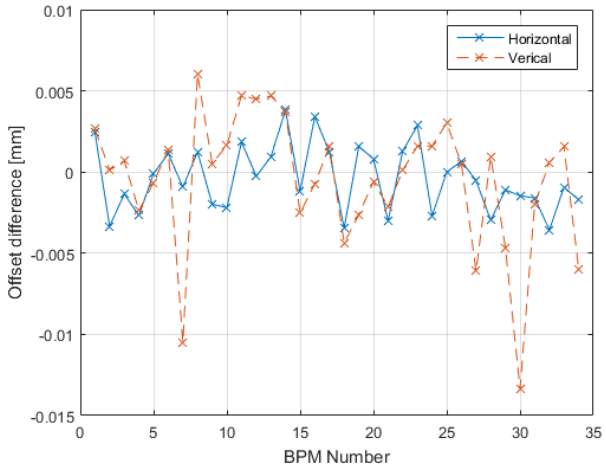

Figure 5.8: Difference in measured offsets depending on the direction of measurement when measuring with correction.

5.2 LOCO

5.2.1 Orbit Response Matrix Measurements

As LOCO bases its calculations on the measured orbit response matrix of the machine it is important that the measurement of the response matrix is as accurate as possible. Initial response matrix measurements did not yield LOCO convergence due to their lack of diagonal symmetry in the lower left quadrant compared to the model (see Figure (5.9)). This quadrant corresponds to the horizontal orbit response given horizontal dipole kicks. Similarly the upper right quadrant corresponds to the vertical orbit response given vertical dipole kicks. The off-diagonal quadrants represent coupling between the horizontal and vertical plane.

The pre-existing orbit response matrix measurement procedure consists of:

1. Applying a positive kick by decreasing the dipole corrector power supply by 10 % of its range
2. Recording the horizontal and vertical beam position in all BPMs
3. Resetting the corrector power supply to its original value
4. Applying a negative kick by increasing the dipole corrector power supply by 10 % of its range
5. Recording the horizontal and vertical beam position in all BPMs
6. Resetting the corrector power supply to its original value
7. The orbit response is calculated as the difference between the two recorded orbits normalised by the dipole corrector strength used

This procedure is repeated for every horizontal and vertical dipole corrector in the machine.

When manually applying a corrector dipole kick to the beam and comparing it to the effect of the same dipole kick in the simulation, it was found that the wiring of the first and last BPM in achromat 12 had been mixed up causing the values reported by the two to be switched. After resolving that issue the orbit response of the machine looked very similar to the model (see Figure 5.11). The vertical response is due to the coupling of the machine, a possible source of which is the beam being vertically offset in the centre of several magnet blocks (see Figure 5.13 and Equation (2.27)). Note that the vertical response is several orders of magnitude smaller than the horizontal. In order to measure a response matrix similar to Figure 5.9b the time delay between setting the dipole corrector kicks and reading from the BPMs had to be increased from 100 ms to 500 ms. This gave the response matrix seen in Figure 5.12.

Power supply tests done at MAX IV included the rise-time of the power supplies (see Figure 5.10). These show that a delay of 100 ms should be enough for the power supply to reach a given current setpoint. However, orbit response matrix measurements indicate that it is not long enough time for the magnet to reach the corresponding magnetic field strength.

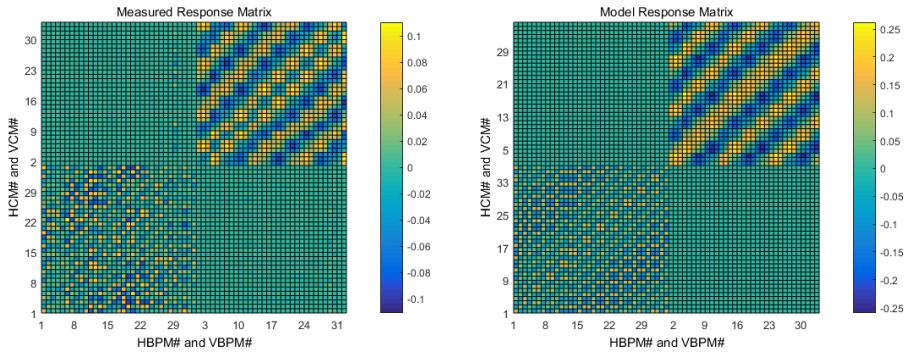

(a) The initially measured orbit response matrix. The lack of systematics was found to be due to the time it took for the dipole corrector magnets to reach the desired field.

(b) The nominal model orbit response matrix. This is used as a starting point for LOCO fits.

Figure 5.9: Initially measured and nominal orbit response matrix.

Due to remanence in the magnets, each time a dipole corrector is reset to its original value after having been altered, the orbit is not the same as initially. This might cause higher order magnetic fields to perturb the orbit response matrix measurement, specifically quadrupole fields arising in the sextupoles (see Equation (2.27)). To correct for this the procedure was modified to include orbit correction:

1. Applying a positive kick by decreasing the dipole corrector power supply by 10 % of its range
2. Recording the horizontal and vertical beam position in all BPMs
3. Resetting the corrector power supply to its original value
4. Correcting the orbit
5. Applying a negative kick by increasing the dipole corrector power supply by 10 % of its range
6. Recording the horizontal and vertical beam position in all BPMs
7. Resetting the corrector power supply to its original value
8. Correcting the orbit
9. The orbit response is calculated as the difference between the two recorded orbits normalised by the dipole corrector strength used

This procedure is repeated for every horizontal and vertical dipole corrector in the machine.

It was not possible to correct the orbit to the BPM offset in every BPM in the vertical plane (see Figure 5.13). The main effect of this is expected to be the skew

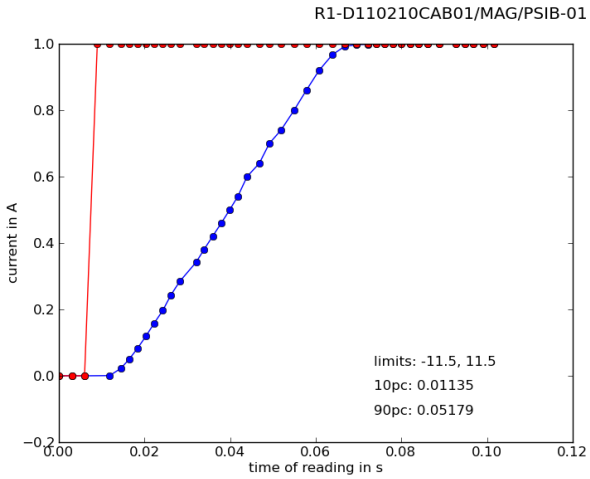

Figure 5.10: Rise-time of one of the dipole corrector power supplies of the 1.5 GeV storage ring. The red line is the digital input signal to the power supply, the blue is the output current of the power supply.

quadrupole field contributions from the sextupoles (see Equation (2.27)). These will be visible in the coupling quadrants of the orbit response matrix.

As both the pre-existing measurement procedure and the modified are capable of producing orbit response matrices similar to the model orbit response matrix, four measurements were done with each procedure. The effect of the orbit correction is investigated when fitting the model to the measured data (see Section 5.2.4).

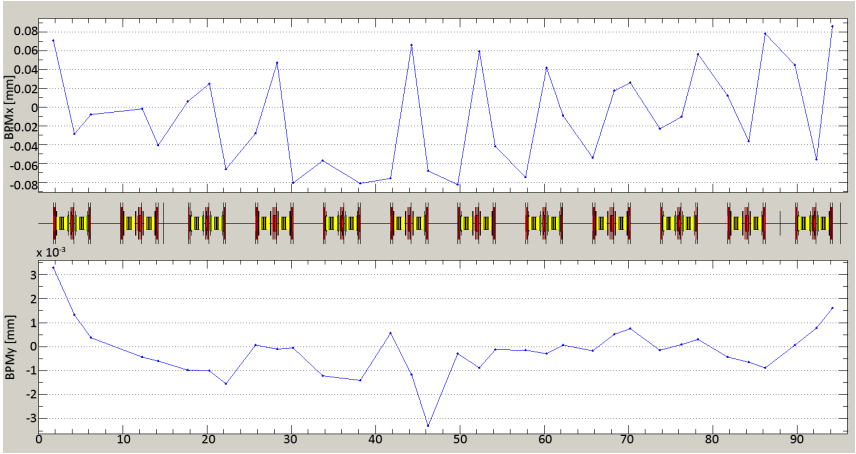

(a) Orbit response of machine when applying a horizontal kick to the beam. The first horizontal corrector was used, with a kick corresponding to 1 A.

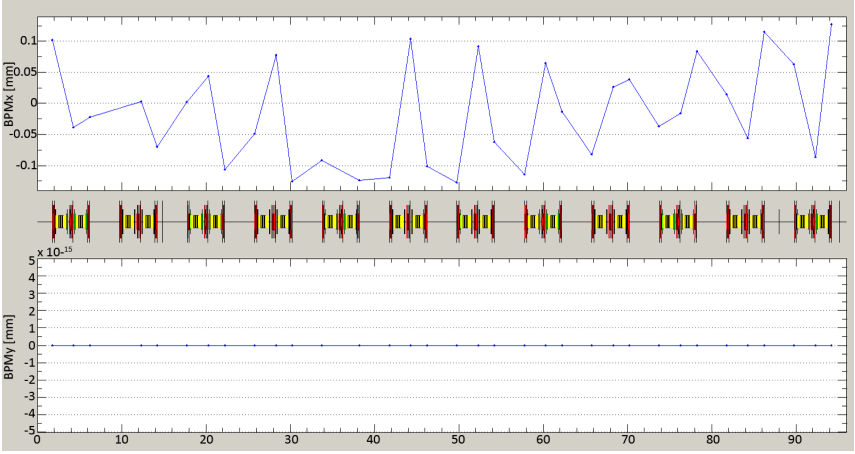

(b) Orbit response of the simulation when applying a horizontal kick to the beam. The first horizontal corrector was used, with a kick corresponding to 1 A.

Figure 5.11: Orbit response of the machine and the simulation given the same dipole kick.

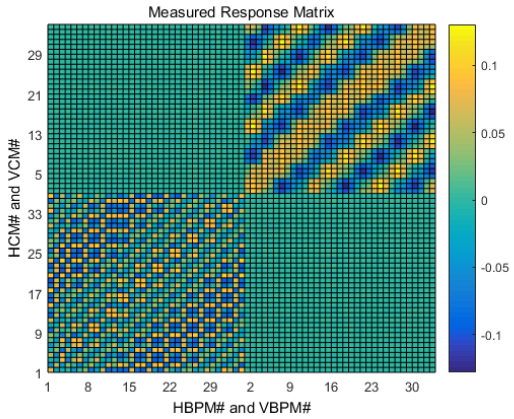

Figure 5.12: Measured orbit response matrix with $500\ \mathrm{ms}$ delay between power supply setpoints and BPM readings.

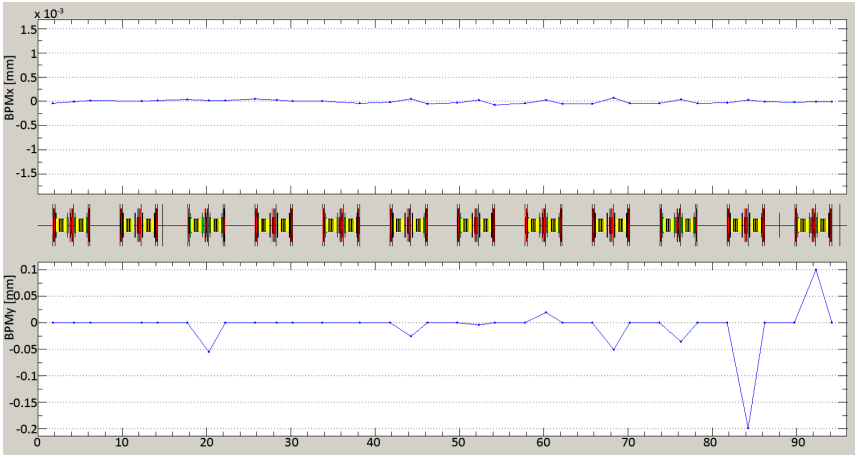

Figure 5.13: Orbit displacement relative to the BPM zero reference. Note that the orbit is not fully corrected vertically.

5.2.2 LOCO Circuit Fits

LOCO was configured to have the option of either fitting the magnet average gradient of the families SQFO, SQFI, and DIP (via the PFS) or fitting the same three families by individual magnet gradient. These are in addition to the options of fitting the corrector magnet kicks, BPM gains, and corrector magnet and BPM coupling. As the families each have a common power supply the individual magnet gradients can only be adjusted through shunting. Since a fit of the magnet average (or circuit fit) is easier to apply these were initially run.

The following measured data was given as input to LOCO:

- Orbit response matrix
- Horizontal dispersion
- Vertical dispersion
- Initial corrector kicks based on field measurements (see Figure 5.14)
- Individual BPM noise

Initially the only parameters to fit were:

- Average gradient of SQFO
- Average gradient of SQFI
- Average gradient of DIP

The average gradients can be adjusted by setting the common power supply of the family. Additionally, all coupling factors were left out of the fit as the only way of currently fitting these would be through the BPM and corrector magnet roll errors, that is, the magnets being slightly rotated around the longitudinal axis. As these coupling terms are the result of manufacturing and alignment, they should be relatively low and are not expected to be responsible for the coupling in the machine. Additionally, it was already known that some of the coupling comes from the vertical position of the beam (see Figure 5.13).

With so few parameters a response matrix fit with low deviation from the measured response matrix was not possible (see Figure 5.15). The residual errors in the response matrix fit can not be corrected by adjusting the average gradient of the magnet families alone.

The circuit fit gave good agreement between the model and machine horizontal dispersion (see Figure 5.16). The vertical dispersion of the machine is due to either coupling or vertical bending fields. As coupling was not included in the fit, no fitting of the vertical dispersion was made.

5.2.3 Applying LOCO Circuit Fits

The results of the LOCO fit were applied to the machine in order to correct the horizontal dispersion closer to the nominal. The application of results is done by linearly scaling the results reported by the LOCO-fitted model:

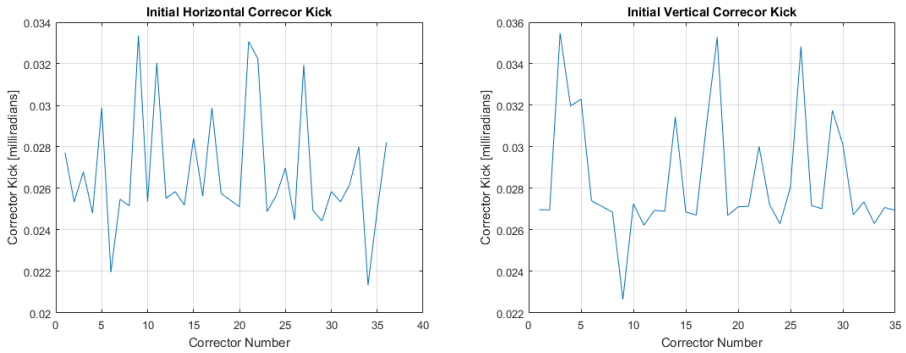

(a) Horizontal dipole corrector kicks. **(b)** Vertical dipole corrector kicks.

Figure 5.14: Dipole corrector kicks based on magnetic field measurements.

$$k_{\text{final}} = k_{\text{goal}} \Big/ \frac{k_{\text{LOCO,final}}}{k_{\text{initial}}} \tag{5.1}$$

where k_{initial}, k_{goal}, and k_{final} are the gradients during the measurement, nominal gradients, and scaled gradients from the LOCO fit respectively. $k_{\text{LOCO,final}}$ is the gradient of the model fitted to the measured data. For instance, if LOCO finds ($k_{\text{LOCO,final}}$) that the model has to have a larger gradient than what the current value represents (k_{initial}) the gradient in the machine is to large. In order to achieve the goal gradient (k_{goal}) the gradient in the machine has to be set to a value (k_{final}) smaller than the goal.

Figure 5.17 shows the resulting dispersion after a single circuit fit applied to the machine. A second iteration of LOCO measurements, fittings, and application to the machine was made in order to further correct the horizontal dispersion. The resulting dispersion after the second LOCO correction can be seen in Figure 5.18, and the corrections done to the magnet families can be seen in Table 5.2. Any shift in beam energy due to the change in dipole bending magnet strength is assumed to be compensated by the PFS which has a dipole component. The tune of the machine after applying each iteration can be seen in Table 5.3.

Iteration	# 0	# 1	# 2
SQFI [T/m]	5.0007	4.9853	4.9737
SQFO [T/m]	5.7237	5.6817	5.6741
PFS [T/m]	−1.3466	−1.3460	−1.3452
BEND [Tm]	−1.3103	−1.3104	−1.3100

Table 5.2: Change in quadrupole gradients and DIP gradient (PFS) and dipole bending field (BEND) from LOCO circuit fits.

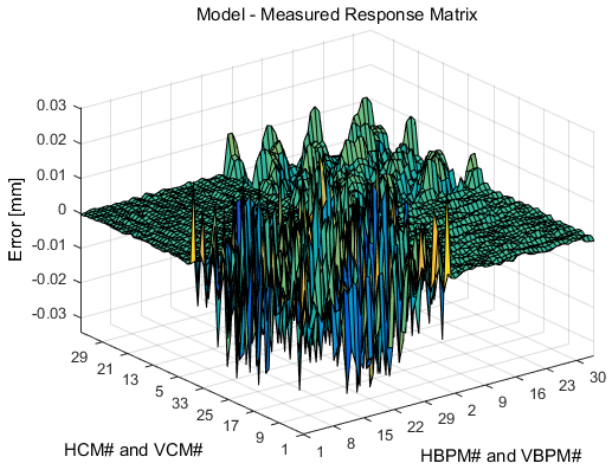

Figure 5.15: Error of orbit response matrix fit when fitting by circuit.

Iteration	# 0	# 1	# 2
ν_h	11.19034	11.2280	11.1729
ν_v	3.2373	3.1645	3.2885

Table 5.3: Tunes of the machine after having adjusted according to the first and second LOCO circuit fit for measured data.

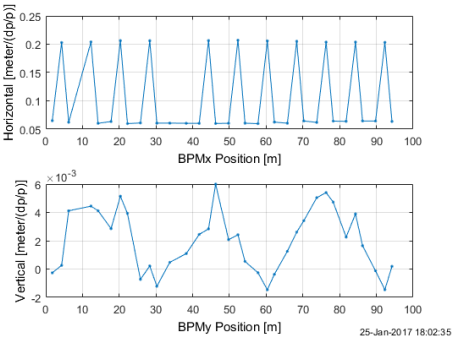

(a) The initial dispersion of the machine. Note the non-zero horizontal values at the valleys. These correspond to the longitudinal positions of the ring where insertion devices are to be placed.

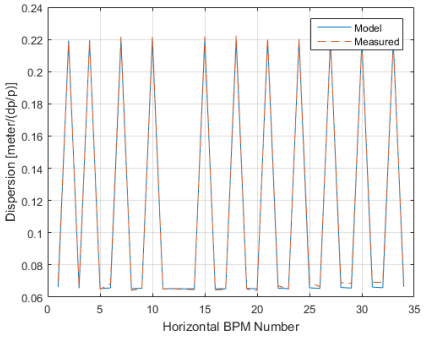

(b) LOCO fit of model to measured horizontal dispersion with the average integrated gradient per magnet in SQFO, SQFI, and DIP as fit parameters.

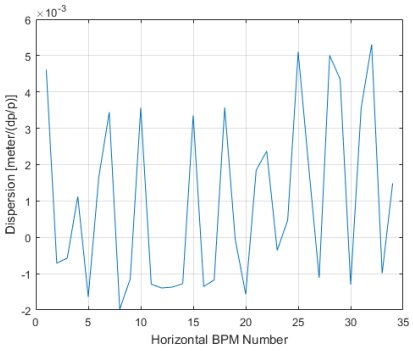

(c) Error of the LOCO fit of the horizontal dispersion.

Figure 5.16: LOCO circuit fit of horizontal dispersion.

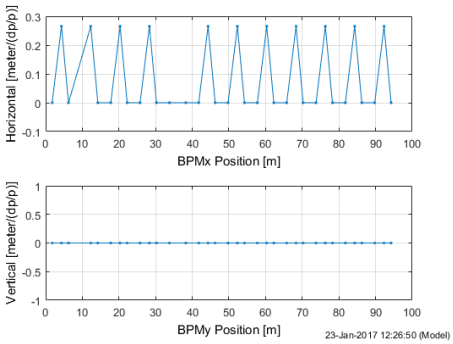

(a) The dispersion of the simulated nominal machine.

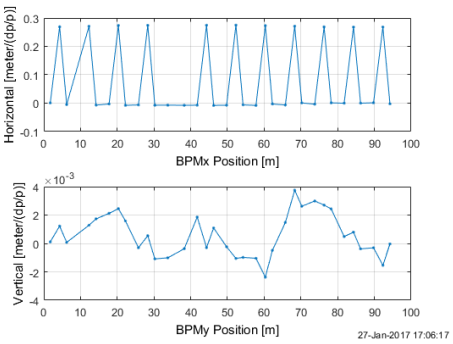

(b) The resulting dispersion after the machine was adjusted according to a one LOCO circuit fit of measured data. Only the horizontal dispersion was fitted. Note that unlike the initial dispersion (Figure 5.16a) the values between the peaks are zero.

Figure 5.17: Horizontal dispersion after applied LOCO fit.

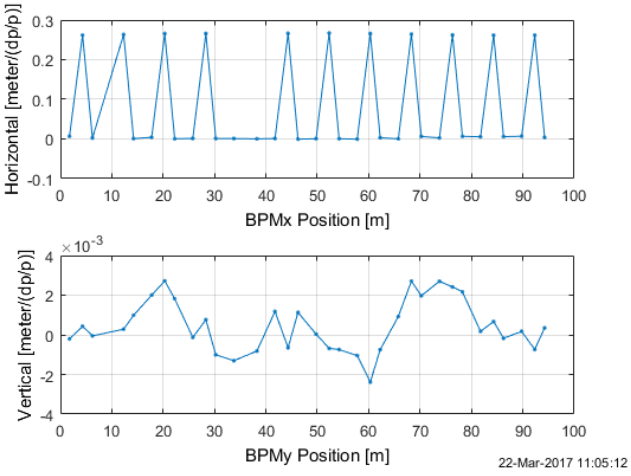

Figure 5.18: The resulting dispersion after the machine was adjusted according to a second LOCO circuit fit of measured data. Only the horizontal dispersion was fitted.

5.2.4 LOCO Magnet Fits

In order to find the beta-functions of the machine, and calculate how individual magnet gradients should be altered to correct the beta-beat LOCO fits by individual magnet gradient were done. Beta-beat is the beating pattern of the beta functions. It occurs when the lattice of a storage ring is not symmetrical. The following measured data was given as input to LOCO:

- Orbit response matrix
- Horizontal dispersion
- Vertical dispersion
- Initial corrector kicks based on field measurements (see Figure 5.14)
- Individual BPM noise

The parameters to fit were:

- BPM Gains
- Corrector magnet kicks
- Individual gradients of SQFO
- Individual gradients of SQFI
- Individual gradients of DIP

Once again the coupling terms were left out of the fit.

In order to assess how much hysteresis effects the end results of the LOCO magnet fit (i.e. the gradient of each magnet which will eventually be used for individual magnet shunting) the model was fitted to four response matrix measurements with correction, and four without (see section 5.2.1).

Uncorrected Orbit Response Matrices

The residual error, when fitting the model to an orbit response matrix measured without correction, can be seen in Figure 5.19. The gradients found by LOCO when fitting to these measurements can be seen in Figure 5.20.

The betatron tunes found by LOCO and the machine tunes at the time of measurement can be seen in Table 5.4.

	$\bar{\nu}_x$	$\bar{\nu}_y$	STD ν_x	STD ν_y
LOCO	11.2294	3.1630	$2.1 \cdot 10^{-5}$	$3.4 \cdot 10^{-5}$
Measured	11.2280	3.1645	$3.2 \cdot 10^{-5}$	$3.2 \cdot 10^{-5}$

Table 5.4: Calculated tunes from LOCO fits without correction.

The dipole corrector kicks and BPM gains found are given in Figure 5.21 and Figure 5.22 respectively.

The beta functions were obtained by fitting the models to the measured data (see Figure 5.23). By comparing these to the nominal beta functions of the model (see Figure 5.24) the beta-beat was found (see Figure 5.25).

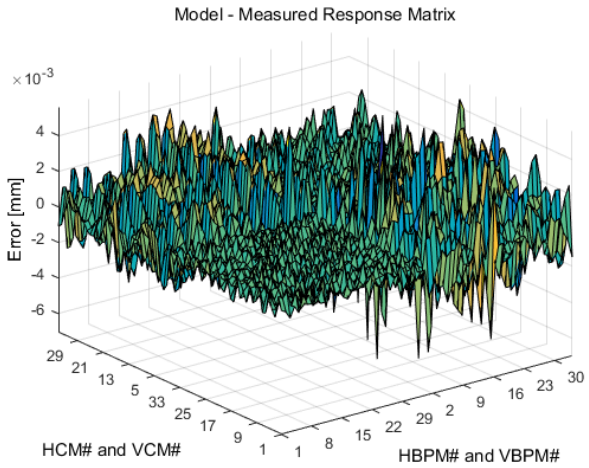

Figure 5.19: Residual error of fit to data measured without correction.

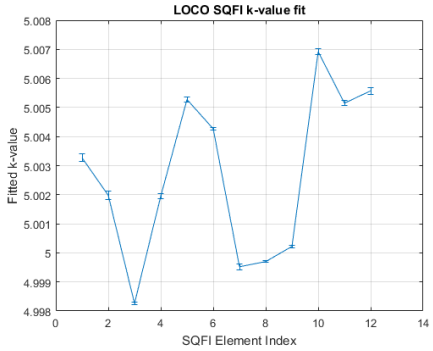

(a) LOCO fitted SQFI k-values using response matrices measured without correction. The error bars represent 2σ of four measurements from 2017-03-13.

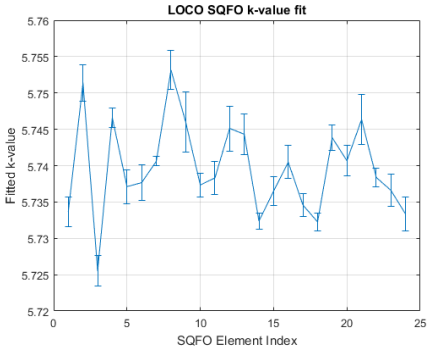

(b) LOCO fitted SQFO k-values using response matrices measured without correction. The error bars represent 2σ of four measurements from 2017-03-13.

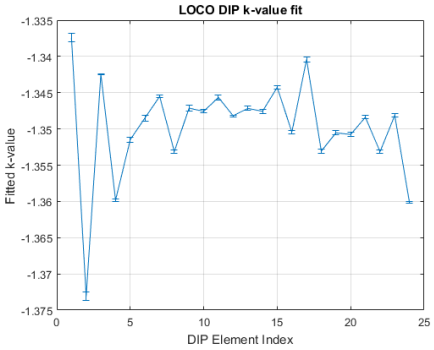

(c) LOCO fitted DIP k-values using response matrices measured without correction. The error bars represent 2σ of four measurements from 2017-03-13.

Figure 5.20: LOCO fitted individual magnet gradients of SQFI, SQFO, and DIP when fitting to orbit response matrices measured without correction.

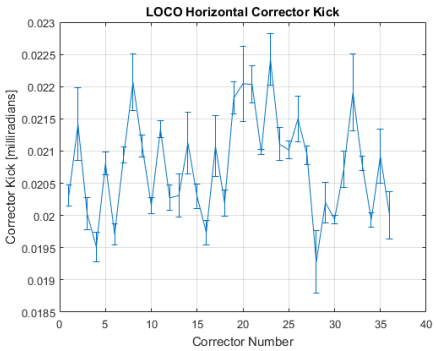

(a) LOCO fitted horizontal corrector kicks using response matrices measured without correction. The error bars represent 2σ of four measurements from 2017-03-13.

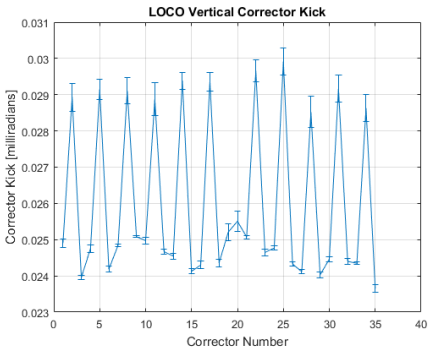

(b) LOCO fitted vertical corrector kicks using response matrices measured without correction. The error bars represent 2σ of four measurements from 2017-03-13.

Figure 5.21: LOCO fitted dipole corrector magnet kicks when fitting to orbit response matrices measured without correction.

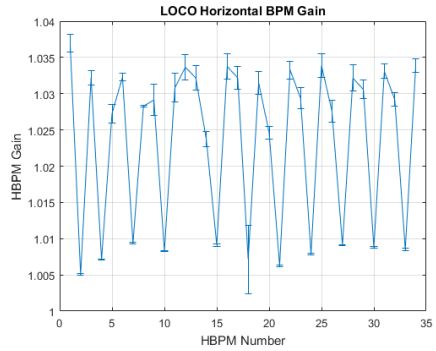

(a) LOCO fitted horizontal BPM gains using response matrices measured without correction. The error bars represent 2σ of four measurements from 2017-03-13.

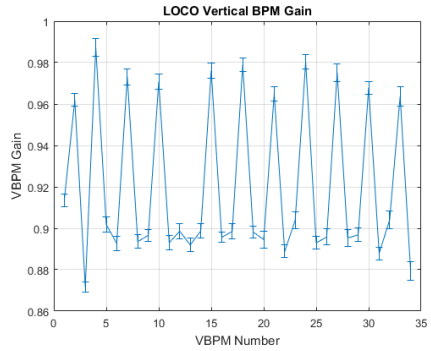

(b) LOCO fitted vertical BPM gains using response matrices measured without correction. The error bars represent 2σ of four measurements from 2017-03-13.

Figure 5.22: LOCO fitted BPM gains when fitting to orbit response matrices measured without correction.

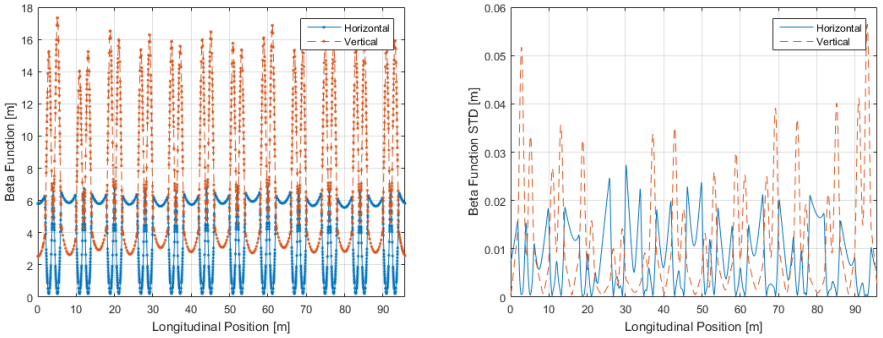

(a) Beta functions of model fitted to four measurements done without correction 2017-03-13.

(b) Standard deviation of beta functions of model fitted to four measurements done without correction.

Figure 5.23: Beta functions of LOCO fitted models.

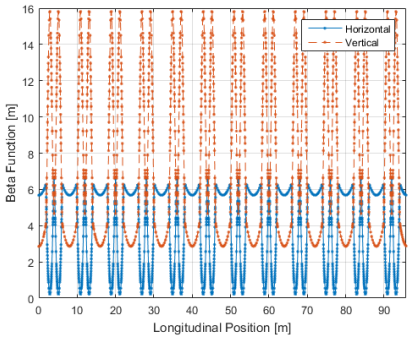

Figure 5.24: Beta functions of nominal AT model.

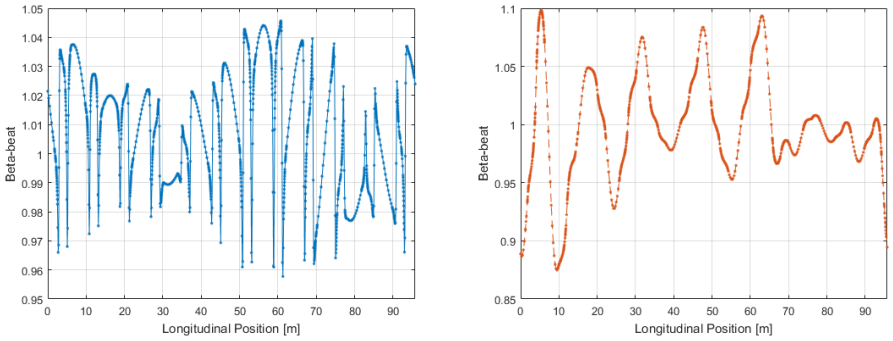

(a) Horizontal LOCO beta function deviation relative model beta function.

(b) Vertical LOCO beta function deviation relative model beta function.

Figure 5.25: Beta-beat of LOCO beta functions.

Corrected Orbit Response Matrices

The residual error of a fit done to an orbit response matrix, measured with correction. can be seen in Figure 5.26. The gradients obtained from several fits are seen in Figure 5.27. Additionally, each gradients effect on χ^2 was calculated (see Figure 5.28).

The betatron tunes found by LOCO and the machine tunes at the time of measurement can be seen in Table 5.5.

	$\bar{\nu}_x$	$\bar{\nu}_y$	STD ν_x	STD ν_y
LOCO	11.2283	3.1636	$9.5 \cdot 10^{-5}$	$2.1 \cdot 10^{-4}$
Measured	11.2280	3.1645	$3.2 \cdot 10^{-5}$	$3.2 \cdot 10^{-5}$

Table 5.5: Calculated tunes from LOCO fits with correction.

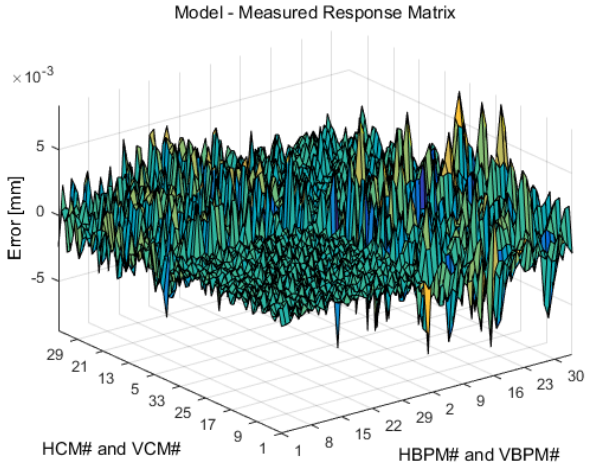

Figure 5.26: Residual error of fit to data measured with correction.

The dipole corrector kicks and BPM gains can be seen in Figure 5.29 and Figure 5.30 respectively. Each separate data set for the vertical corrector kicks and BPM gains can be seen in Figure 5.31

The beta functions were calculated from the fit of the models to the measured data (see Figure 5.32). As the beta-beat of these fits is very similar to that of the fits done on uncorrected measurements it will not be plotted.

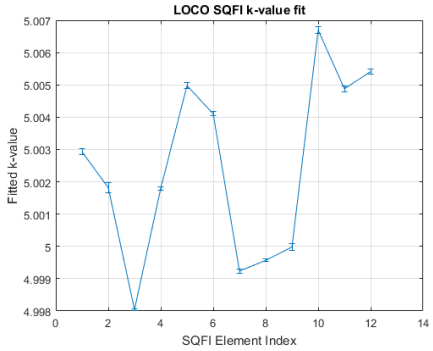

(a) LOCO fitted SQFI k-values using response matrices measured with correction. The error bars represent 2σ of four measurements from 2017-03-17.

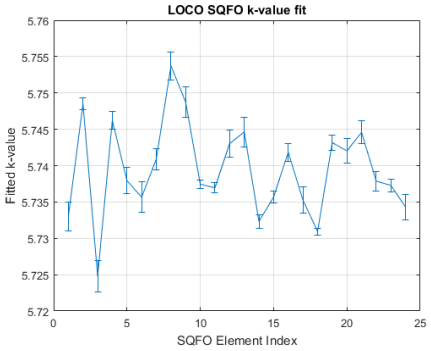

(b) LOCO fitted SQFO k-values using response matrices measured with correction. The error bars represent 2σ of four measurements from 2017-03-17.

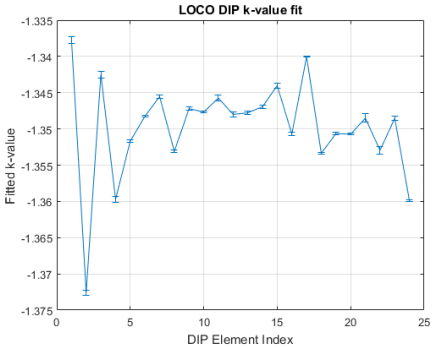

(c) LOCO fitted DIP k-values using response matrices measured with correction. The error bars represent 2σ of four measurements from 2017-03-17.

Figure 5.27: LOCO fitted individual magnet gradients of SQFI, SQFO, and DIP when fitting to orbit response matrices measured with correction.

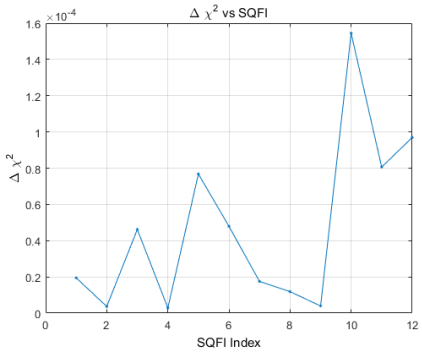

(a) χ^2 sensitivity to changes in the SQFI gradients.

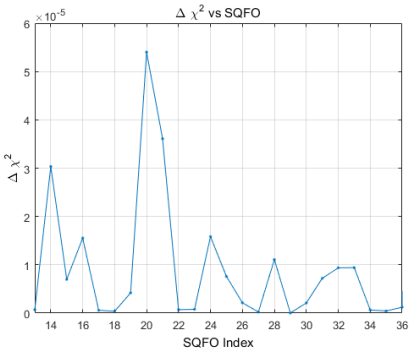

(b) χ^2 sensitivity to changes in the SQFO gradients.

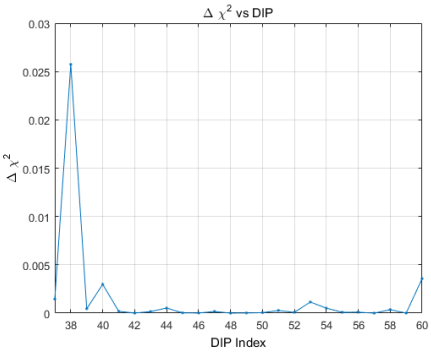

(c) χ^2 sensitivity to changes in the DIP gradients.

Figure 5.28: Sensitivity of χ^2 depending on the fitted magnet gradients.

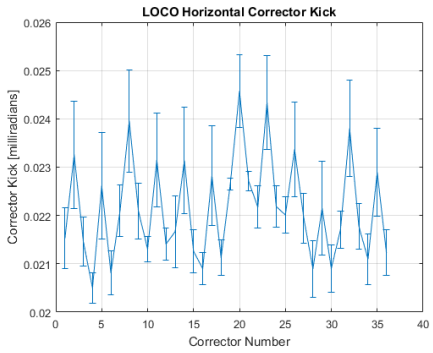

(a) LOCO fitted horizontal corrector kicks using response matrices measured with correction. The error bars represent 2σ of four measurements from 2017-03-17.

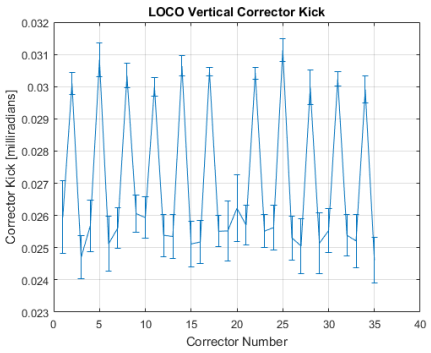

(b) LOCO fitted vertical corrector kicks using response matrices measured with correction. The error bars represent 2σ of four measurements from 2017-03-17.

Figure 5.29: LOCO fitted dipole corrector magnet kicks when fitting to orbit response matrices measured with correction.

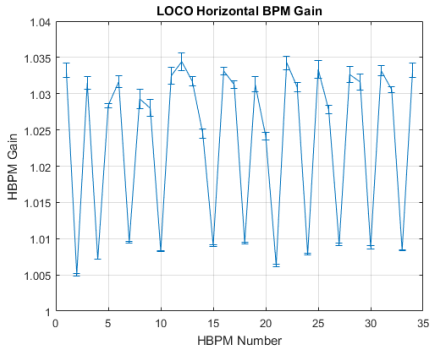

(a) LOCO fitted horizontal BPM gains using response matrices measured with correction. The error bars represent 2σ of four measurements from 2017-03-17.

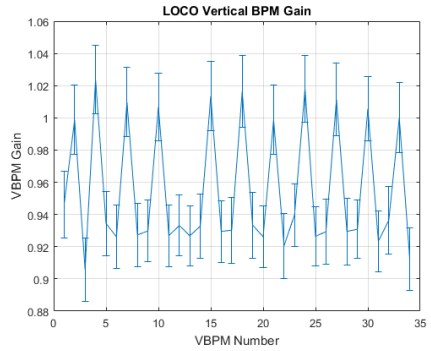

(b) LOCO fitted vertical BPM gains using response matrices measured with correction. The error bars represent 2σ of four measurements from 2017-03-17.

Figure 5.30: LOCO fitted BPM gains when fitting to orbit response matrices measured with correction.

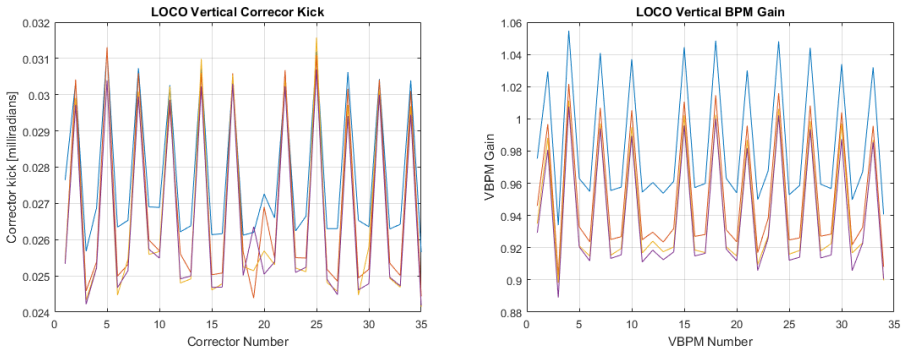

(a) LOCO fitted vertical dipole corrector kick of four measurements from 2017-03-17 measured with correction.

(b) LOCO fitted vertical BPM gain kick of four measurements from 2017-03-17 measured with correction.

Figure 5.31: The vertical BPM gains and corrector kicks found by LOCO through fitting the data measured with correction. Since the vertical dispersion was not included in the fit the ratio between the vertical corrector kicks and BPM gains could not be reliably determined.

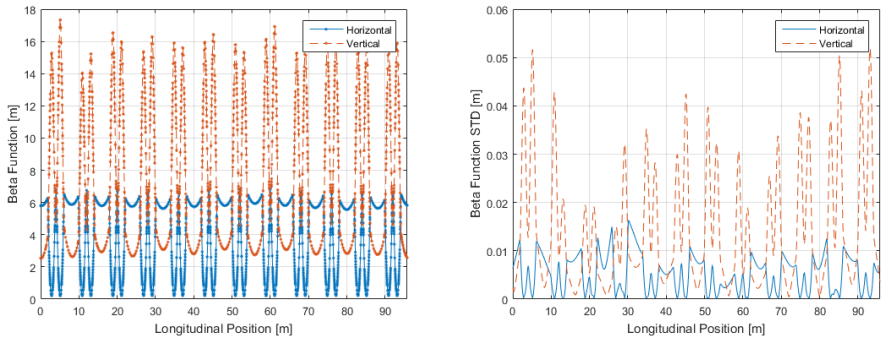

(a) Mean beta functions of model fitted to four measurements done with correction 2017-03-17.

(b) Standard deviation of beta functions of model fitted to four measurements done with correction.

Figure 5.32: Beta functions of LOCO fitted models.

5.2.5 Applying LOCO Magnet Fits

The LOCO fits by magnet was applied by increasing the power supply output current to the point where the weakest individual magnet, reported by LOCO, had nominal strength. The strength of the remaining magnets, which are now stronger than nominal, can be individually decreased by connecting an appropriate resistance in parallel with the main coil of the magnet (see Figure 3.3). The procedure for measuring the main coil resistances can be found in Section 5.3 and the resulting resistances in Appendix C.

The shunt board are safe to use at a heat load of 1 W over a single resistor. This corresponds to a temperature of 70°C. At 2 W the solder was known to melt. Resistance calculations showed that the magnet families SQFI and SQFO would result in too high a heat load over the resistors. Thus, attempts to correct individual magnet errors were only done on the DIP family. Despite calculations showing that the heat load over each DIP resistor used would be less than 1 W the shunt board showed hot-spots at over 110°C. The shunting was removed, and the attempt aborted.

5.3 Tune-Shift Measurements

The spectrum analyser was set up so that it had a resolution of 100 Hz. Using Equation (3.8) this was found to correspond to a fractional tune measurement resolution of $\sim 3.2 \cdot 10^{-5}$.

The tune-shift measurements only give information regarding the beta functions of the machine and, unlike LOCO, nothing about how to correct for beta-beat. Because of this the tune-shifts are intended to be used as an independent measurement of the beta functions in order to assess the trustworthiness of the LOCO fits.

The tune-shift is achieved by shunting one of the quadrupoles using the relay controlled shunt resistance. This decreases its focusing gradient by a small fraction, after which the change in tune can be measured. Due to hysteresis, setting the shunt to off will not fully restore the field of the quadrupoles. This small change in gradient leads to different optics and beta functions in the machine. In order for all measurement points to be done on the same optics the ring has to be cycled between each point. As this is very time consuming, 20 minute cycling time followed by reinjection and correction of the beam, and requires a lot of access to the linac, a different approach was chosen.

By repeatedly setting the shunts to on and off a new hysteresis loop was established in the quadrupoles. This allows all measurement points to be taken on the same optics and beta functions. As the establishing of a new hysteresis loop causes the beta functions to change a new dispersion and orbit response matrix measurement with correction was also taken. This is later to be used when comparing the tune-shift beta functions to those reported by LOCO.

As the vertical tune peak in the spectrum analyser was not well defined enough for measurements of sufficient accuracy, the tune-shift measurements were only done in the horizontal plane.

Figure 5.33 shows the tune-shift and standard deviation of five separate measurements. In the interest of time, the ring was not cycled between each full measurement.

Equation (4.5) was used to calculate the mean beta function in the quadrupoles. The Δk term was found by measuring the voltage over each individual quadrupole magnet at its connection to the shunt board (see Figure 5.34). The measurements were done both with and without the corresponding relay controlled shunt resistance connected. This measurement arrangement includes the effect of cabling to and from the resistances. As the cables accounted for a significant portion of the resistance, and were of varying length from one magnet block to another, it was deemed that theoretically calculating the effect of the cables would not give sufficient accuracy. The measured resistances can be found in Appendix C.

Initial voltage measurements found that the voltage over the quadrupoles was ~ 6.3 V for the SQFO family and ~ 11.3 V for the SQFI family. The shunts were found to decrease the current through the magnet coils by very close to 1 % for all magnets. In order to resolve the beta-beat of the machine, which is on the order of a few percent, the voltage measurements need to be accurate to at least $1 \cdot 10^{-4}$. This is essentially the accuracy limit of this measurement arrangement due to magnet power supply noise. Due to measurement difficulties it was only

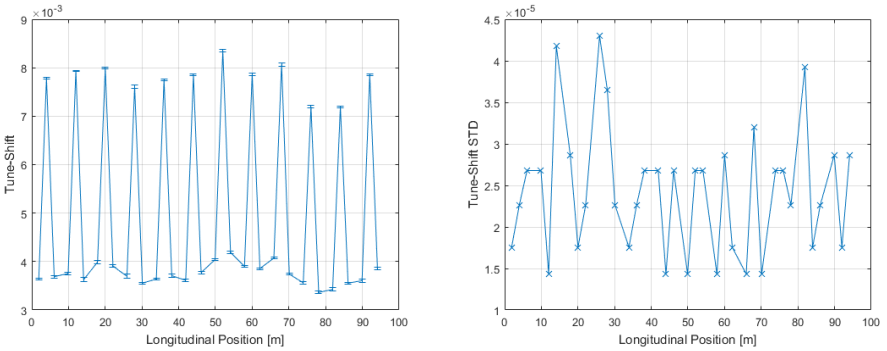

(a) Tune-Shift when shunting SQFO and SQFI magnets. Note that a hysteresis loop was established before measuring. The error bars represent 2σ of five measurements taken 2017-03-20.

(b) Standard deviation, σ, of five tune-shift measurements taken 2017-03-20.

Figure 5.33: Tune-shift when shunting the magnets of the families SQFO and SQFI.

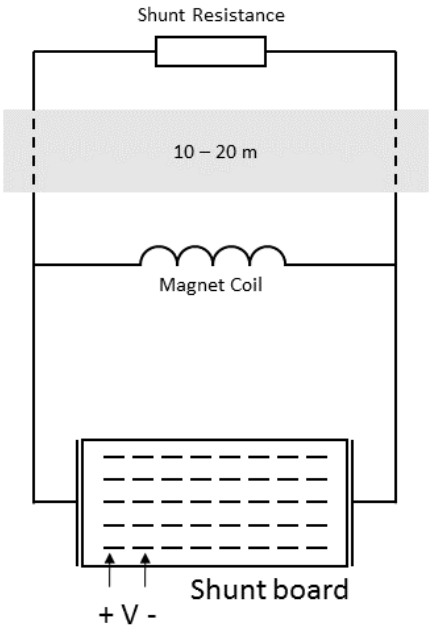

Figure 5.34: Voltage measurement setup used to find the resistance of the shunts.

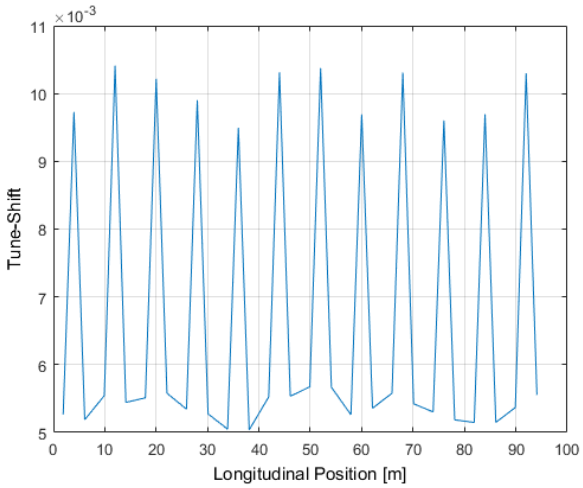

Figure 5.35: Tune-shifts of the model.

SQFI decrease	0.1 %	0.5 %
Model	0.01159	0.05686
Machine	0.01206	0.05501

Table 5.6: Changes in tune when decreasing the SQFI power supply in the simulator as well as the machine.

possible to reach an accuracy of $\sim 2 \cdot 10^{-4}$.

By decreasing the strength of the quadrupoles in the model by a fraction determined by the measured shunt resistance of the corresponding magnet in the machine the same measurement could be done on the model. The tune-shifts of the model can be seen in Figure 5.35 and the calculated beta values of both the model and the machine can be seen in Figure 5.36. As there was a significant difference between the model and machine values the models ability to predict shifts in tune was investigated by decreasing the SQFI gradient in both the machine and the model (see Table 5.6).

In addition to the full tune-shift measurement campaigns, a few measurements were done without using the shunts to preemptively establish a hysteresis loop. Instead the entire ring was cycled between each measurement. The results of these measurements can be seen in Table 5.7.

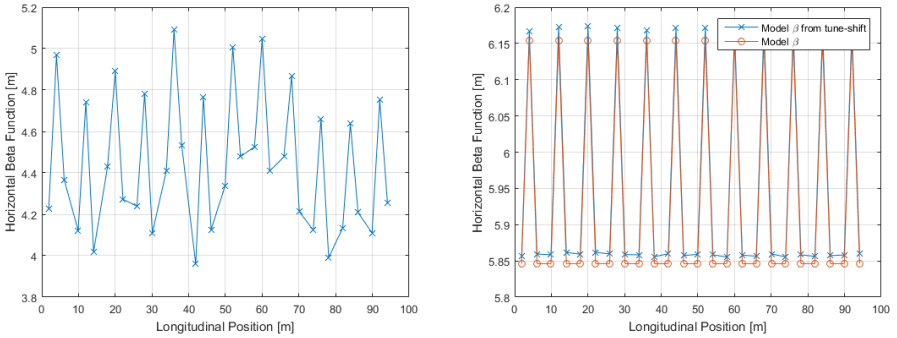

(a) Beta values from tune-shift measured on the machine.

(b) Beta values from tune-shift measured in the simulator compared to the actual model beta functions.

Figure 5.36: Horizontal beta values from tune-shift measurements.

SHUNT	$\beta_{x,\text{tune-shift}}$ [m]	$\beta_{x,\text{LOCO}}$ [m]
[1 1]	4.5961	5.8452
[1 2]	5.3163	6.3528
[1 3]	4.5037	6.0696
[6 1]	4.8522	5.8147
[6 2]	5.6236	6.2615

Table 5.7: Calculated beta function values from tune-shift measurements without cycling the shunts.

Chapter 6
Discussion

6.1 BPM Offsets

6.1.1 Uncorrected Measurements

The uncorrected measurements show the highest standard deviation, and thus the worst reproducibility of all investigated measurement methods. This does not appear to be due to insufficiently establishing a hysteresis loop using the shunts. The loop was established by setting the shunts on and off for five iterations, which according to tune measurements is sufficient to establish a fairly well defined hysteresis loop (see Figure 5.3). The reproducibility is rather due to the measurement procedure changing the initial beam position throughout the measurement. The change in beam position occurs both because of dipole corrector remanence, and the establishing of a hysteresis loop changing the optics throughout the measurement. The change in optics will lead to a change in beam position for every quadrupole in which the beam is not centred, as is the case in the vertical plane for several quadrupoles (see Figure 5.13). Additionally the dipole corrector remanence will further displace the beam. The combined beam displacement of both these effects leads to the beam being experiencing non-linear effects, such as the effects from sextupole magnets. As the offset measurement methods is based on the linear effects of the quadrupole magnets, higher order terms will negatively effect the measurements.

The effect of the change in optics can also be seen in Figure 5.2. When measuring the offset of a given BPM the optics of the ring will be different depending on the order of which the BPM offsets are measured. As discussed above, this will affect the value found by the measurement. Ideally the BPM offset measurement procedure should result in the same values regardless of in what order the measurement points are taken.

6.1.2 Preemptively Established Hysteresis Loop

The change in optics which occurs when measuring offsets using the uncorrected measurement method can be accounted for by preemptively establishing the relevant hysteresis loop on all the quadrupoles to be used in the measurement. Note that the beam is corrected after establishing the loop.

The new hysteresis loop on the quadrupoles mean that quadrupole remanence will not effect the measurement; no change in optics will occur from one measurement point to another. Any change in orbit during the measurement is likely due to dipole corrector hysteresis. This is reflected in the standard deviation when comparing several complete measurements (see Figure 5.4b). Both the horizontal and vertical reproducibility of measurements done after preemptively establishing a hysteresis loop are better than that of the pre-existing measurement procedure. As the beam is still significantly displaced in the vertical plane and is further displaced by dipole corrector hysteresis, there are still higher order magnetic field effects. However, the higher order effects seem to affect each complete measurement set in a similar way, as the reproducibility of both the horizontal and the vertical offsets are similar (despite the vertical displacement being much larger).

As the optics do not change during the measurement when using the preemptively established hysteresis loop measurements done in the order achromat 1 to 12 are more similar to a measurement done in the order 12 (see Figure 5.5). Compared to the uncorrected measurements the difference seems to have decreased by a factor of 2 to 3. The large horizontal difference seen in BPM 17 might be due to a higher sensitivity to the strength of the dipole correctors in that point, which in turn means that this point is more sensitive to dipole corrector hysteresis.

6.1.3 Corrected Orbit and Preemptively Established Hysteresis Loop

BPM offset measurements after preemptively establishing a hysteresis loop and using orbit correction between each measurement point were done in order to correct for both quadrupole and dipole corrector hysteresis. The standard deviation of this measurement was found to be $< 1\,\mu m$ in the horizontal plane, but significantly higher, maximum at $5\,\mu m$, in the vertical plane (see Figure 5.6b). The vertical standard deviation is higher than for the measurements not using orbit correction. This might be due to the correction not being able to correct the vertical beam position in several BPMs (see Figure 5.13). The vertical position in these BPMs will instead drift, and is thus different for each measurement. It is possible that this drift is increased by the orbit correction which would explain its negative impact on the vertical reproducibility of the measurement.

For the BPMs which could not be corrected vertically, a vertical offset was set to the beam position. When correcting the beam, the vertical position of the orbit was not corrected to a value corresponding to the zero reference of these BPMs, but rather to the larger reference value which the dipole correctors had enough strength to correct to. This means that each measurement point is done on the same orbit. This addition lowered the vertical standard deviation of the measurement (see Figure 5.7b), which confirms that the the lower reproducibility was at least partly due to the inability to vertically correct the beam in some BPMs. Despite this the reproducibility of the vertical offset is still worse than the horizontal. The remaining discrepancy might be due to the measurement being more sensitive to changes in orbit when the orbit is already offset. The orbit correction will reduce the orbit displacement to roughly BPM noise levels ($\sim 0.3\,\mu m$). This error seems to have a greater impact on the measurement when the orbit is already displaced (as it is in the vertical centre of many of the achromats). The vertical reproducibility

can likely be improved to the level of the horizontal if it was possible to fully correct the vertical orbit.

The same behaviour can also be seen when measuring the BPM offsets in different directions (Figure 5.8) where the horizontal difference is small but the vertical is significantly larger.

6.2 LOCO

6.2.1 LOCO Circuit Fits

When fitting only the average field gradient of the magnet families SQFO, SQFI, and DIP it was not possible to get a sub-micron standard deviation of the residual error between the measured and fitted model response matrix (see Figure 5.15). This is not surprising as it is not possible to represent individual magnet errors with the magnet family average. In order to reduce the beta-beat, individual magnets need to be corrected.

No attempt was made to fit the coupling terms, as the priority was to correct the linear optics prior to coupling.

The circuit fit of the horizontal dispersion was fairly good. Looking at Figure 5.16c there is still some error between the LOCO fitted model and the measured data. This error is likely due to individual magnet field errors, mainly errors in the bending dipoles and quadrupoles as these are the main contributors to the horizontal dispersion. The error of the circuit dispersion fit is small, which indicates that the gradient errors of the dipoles and quarupoles are also small.

6.2.2 Applying LOCO Circuit Fits

Comparing the horizontal dispersion after the first and second LOCO fit was applied to the machine (see Figure 5.17 and 5.18 respectively) the second iteration only shows a very slight change in the dispersion compared to the first. This is also reflected in the decreasing change in gradients found by LOCO (see Table 5.2).

As only the horizontal dispersion was fitted when fitting the measured data by circuit no other parameters can be expected to converge towards the nominal. This is the case for the betatron tune of the machine (see Table 5.3). As the change in gradient between the first and second LOCO iterations are small compared to the change between the initial values and the first LOCO iteration the values were deemed to have sufficiently converged. Additionally the tunes of the machine are close to nominal (horizontal 11.2200, vertical 3.1500) after the first iteration. No further LOCO circuit fits were applied to the machine.

6.2.3 LOCO Magnet Fits

The residual error of the response matrix fit when fitting by magnet was significantly smaller compared to the circuit fit (see Figure 5.19 and Figure 5.26). The horizontal and vertical orbit response error is essentially at BPM noise levels, with

little or no systematics remaining. As no skew quads were included in the fit the model orbit response matrix coupling quadrants could no be fitted.

As the resulting magnet gradients from the LOCO magnet fits were to be used for correcting individual magnet field errors the reproducibility of the measurement and LOCO fit is important. Initial measurements showed good reproducibility for most fit parameters. However the gradient of the SQFO magnets showed poor reproducibility compared to the other two magnet families (see Figure 5.20b). The gradient value of the second bending dipole (see Figures 5.20c and 5.27c) was shown to deviate from significantly from the mean. This might be due to gradient errors in other magnets in the second half of achromat one. LOCO takes these errors into account when fitting and attributes them to the magnets it is allowed to fit. This is not necessarily a problem as long as it is possible to correct the beta-beat using the fitted gradients. This way of correcting machine optics is already done at other labs.

The fitted dipole corrector magnet kicks and BPM gains (see Figures 5.21 and 5.22) showed individual deviations, small enough to be considered reasonable. The spikes observed in the BPM gains could be due to the different structure in the centre of each magnet block compared to the ends and the difference in BPM structure (see Figure 3.4). Similar spiked structure can also be seen in the dipole corrector kicks despite it not being present in the measured magnetic fields (see Figure 5.14). A possible explanation could be that the pattern arises from the shape of the beta functions, as the response of the beam from a dipole kick depends on both the strength of the magnet and the value of the beta functions at the position of the magnet (see Equation (8.4)). This is interpreted by LOCO as differing kick strengths. Another explanation could be that the skew quadrupole components in the machine give rise to a ringing pattern in the horizontal and vertical plane, which is attributed to the dipole kicks as no skew quadrupoles are included among the fit parameters.

Measurements, with and without correction, lead to almost exactly the same beta functions (see Figure 5.23 and Figure 5.32). Measurements with correction give beta functions with higher horizontal reproducibility. The vertical reproducibility does not seem to be improved. The lack in improvement might be due to the inability to correct the beam vertically in all BPMs. The displaced beam in these BPMs seems to have a greater effect on the measurement than dipole corrector remanence.

When measuring the orbit response matrix with correction the reproducibility of the found SQFO gradient was somewhat improved (see Figure 5.27b). Additionally, the found horizontal corrector kicks were somewhat different.

The lower reproducibility of the SQFO gradients can be explained by looking at χ^2's sensitivity to the different individual gradients (see Figure 5.28). The more sensitive χ^2 is to changes in a gradient the more accurately and consistently it will be determined by the LOCO fit. The reproducibility of the SQFO gradients is not necessarily an issue as gradients which have little effect on χ^2 will likely not need to be as accurately set when correcting the beta beat in the real machine.

As the BPM gains and dipole corrector kicks both alter the amplitude of the orbit response matrix LOCO needs additional inputs to determine the ratio between gains and kick strengths. This is done through the dispersion fit, as

it depends on the BPM gains but not the corrector magnet kicks. The vertical dispersion was likely caused by skew quadrupole fields present due to the large vertical displacement in several sexupole magnets. As no coupling terms were included among the fit parameters this could not be fitted. Thus, there was no way of determining the ratio between the vertical BPM gains and correction kicks. The effect of this can be seen in Figure 5.31.

6.2.4 Applying LOCO Magnet Fits

Despite heat load calculations reporting a heat load of < 1 W the resistors used to shunt the DIP magnet family were heated to $> 100°$C. As this ran the risk of melting the solder, the decision was made to remove the shunting. The cause of the extra heating is likely the small distance between each resistor. When shunting the DIP family, several of the higher resistance resistors were used in parallel. As these are positioned only a few millimetres from one another the resulting heat load on a small area of the shunt board is significantly higher than 1 W (roughly $1.4 - 1.6$ W), despite the individual resistors experiencing a heat load < 1 W. The combined heat load results in temperatures too high for the board.

The inadequacy of the magnet block shunt boards is a known issue at MAX IV, and these tests confirm the issue. At the Polish light source SOLARIS, which houses an identical ring to the 1.5 GeV storage ring, a solution to the heating has been devised. The intention is to copy this solution and implement it on the 1.5 GeV storage ring. At the writing of this report this has not yet been done.

6.3 Tune-Shift Measurements

The accuracy of the tune-shift measurements was limited by several factors. The resolution of the tune measurements and resistance measurements introduce an error of ~ 3 % each. Furthermore Equation (4.5) assumes a small perturbation to the magnet gradient. According to the simulations a perturbation of ~ 1 % will yield values within ~ 3 % of the beta functions (see Figure 5.36b). A smaller perturbation will give more accurate results, but will in turn be more difficult to measure on the actual machine.

The beta function values calculated from the tune-shift measured after preemptively establishing a hysteresis loop using the shunts had an amplitude ~ 20 % smaller than what was expected from the model beta functions. This is partly due to the unknown hysteresis curve in the quadrupoles. Despite this, there appears to be some indication of the same beta-beat pattern in both the tune-shift measurements and the beta functions reported by LOCO (see Figure 6.1a). This can be seen more clearly by scaling the beta values with a common scaling factor for each magnet family (see Figure 6.1b). The pattern indicates that the measurement technique can resolve some details regarding the beta values, but with a large unexpected offset.

Only a few points were measured without preemtively establishing a hysteresis loop using the shunts (see Table 5.7), and therefore were measured with quadrupoles on a known hysteresis curve. The reported beta values were of a

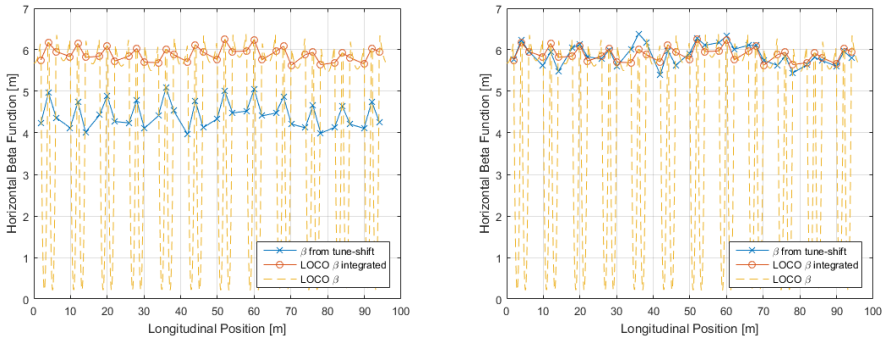

(a) Horizontal beta function calculated from tune-shift compared to LOCO.

(b) Scaled horizontal beta function calculated from tune-shift compared to LOCO.

Figure 6.1: Horizontal beta function from tune-shift measurements and LOCO fit.

somewhat higher amplitude, but still significantly lower than the nominal beta function values (see Figure 5.24).

The tune-shifts from the relay controlled shunts in the model was significantly higher than in the real machine (see Figure 5.35). Despite this the model was able to accurately predict changes in tune of similar magnitude when changing the setpoint of the power supplies (see Table 5.6). This is an indication that there is a problem with the technical implementation of the relay controlled shunts in the real machine. Further investigation is required before these values can be considered trustworthy.

Chapter 7
Conclusions

7.1 BPM Offsets

Investigations of the offset measurement procedure showed that the measured offsets were affected by magnet hysteresis from both the quadrupoles and dipole correctors. These effects lead to a decrease in accuracy and reproducibility of the measurement procedure. The quadrupole hysteresis was accounted for by properly establishing a hysteresis loop prior to the measurement. This decreased the standard deviation between measurements by a factor of two. Additionally it also decreased the effect the order of the measurement had on the results.

By correcting the orbit between measurement points it was possible to improve the horizontal offset measurements further. The standard deviation was decreased to the level of BPM noise (which is at $\sim 0.3\,\mu m$), while the difference between measurement direction was $< 2\,\mu m$ for all BPMs. As it was not possible to vertically correct the beam to a zero reference orbit in several BPMs, the orbit correction initially negatively impacted the measurement. This was partly resolved by instead correcting to a non-zero reference in those BPMs. The vertical BPM offset measurements would likely also be limited by only the BPM noise if it was possible to fully correct the beam vertically.

As the MAX IV lattices were designed with a BPM offset reproducibility of $3\,\mu m$ in mind[20] this method yields more than sufficient results for the BPM offsets.

7.2 LOCO

By fitting the AT model to measured data from the machine it was possible to find the average magnet gradients which would bring the horizontal dispersion closer to the nominal. Applying these to the machine had the expected results as the horizontal dispersion was brought much closer to the nominal. In the process the horizontal and vertical tune was also improved. Only a single iteration was required to correct the horizontal dispersion. Applying a second iteration did not improve the dispersion pattern further, but resulted in tunes further from the nominal. This is not surprising as the tunes were not explicitly a part of the fit.

The vertical dispersion is a result of coupling and vertical dipole bending fields.

As neither of these were parameters in the LOCO fit the vertical dispersion was not corrected.

LOCO fits by individual magnet gradients were done using orbit response matrices measured both with and without orbit correction. The orbit correction slightly improved the reproducibility of the individual magnet gradients, in particular the SQFO gradients.

Unfortunately it was not possible to correct the 1.5 GeV storage ring optics by individually adjusting magnet gradients. The heat load was too large in the shunt resistances designed for this purpose. The inadequacy of the shunt resistance circuit boards was a suspected issue prior to this investigation, and are now to be replaced by a more heat resistant design.

7.3 Tune-Shift Measurements

It turned out to be difficult to extract the beta functions from the shifts in tune which arise when modulating the strength of the quadrupoles. Simulations showed that the error in this type of measurement is ~ 3 % when decreasing the quadrupole strength by ~ 1 %. In addition to this, resistance and tune measurements could only be done with an error of ~ 3 %, which is not not enough to accurately resolve the horizontal beta-beat. Due to the vertical tune peak in the spectrum analyser not being well defined enough, tune-shift measurements could not be done in the vertical plane.

In addition to the measurement inaccuracies the beta function calculated from the tune-shift also reported an amplitude $\sim 10 - 15$ % lower than expected. This systematic error is yet to be discovered, but a similar issue was found when using this beta function measurement method at SOLARIS[19]. Despite this, the technique reports a similar beta-beat pattern to that of LOCO.

7.4 Summary

- A procedure for measuring BPM offsets which gives reproducible results within 3 µm has been developed. Additionally, the procedure is able to give results reproducible within BPM noise in the horizontal plane. The reproducibility in the vertical plane can likely be improved to the same level once the beam can be fully corrected in the vertical plane.
- Unfortunately no correction of the beta-beat could be done. This was due to the shunt resistance circuit boards designed for this purpose could not withstand the generated heat load. This design flaw needs to be rectified before any correction of the beta-beat can be done.
- Due to a yet to be discovered systematic error of $\sim 10 - 15$ % it was not possible to measure the beta functions of the machine using the tune-shift measurement procedure. The error is currently suspected to be a result of the technical implementation of the relay controlled shunts.

Chapter 8

Future Work

Based on the results of this work, some suggestions regarding future research and projects can be made:

- The BPM offset measurements are already within the reproducibility target based on the lattice design[20]. Further improvements could be possible once the vertical beam position can be corrected in all BPMs.
- The shunt resistance circuit boards of the 1.5 GeV storage ring need to be replaced before any corrections of the beta-beat can be done. The new shunt boards need to be able to withstand a higher heat load.
- In order to be able correct coupling LOCO needs to be configured to fit individual skew quadrupole gradients. As the correction would be done in the same way as the beta-beat correction it will likely rely on the new shunt boards being present.
- LOCO could also be configured to fit the rotation of the magnet blocks. This might make it possible to correct some aspects of the optics without altering the individual magnet currents.
- The effects the relay controlled shunts have on the fields of the magnets need to be further investigated. Suggest investigating how a sudden decrease in circuit resistance effects the power supply current output.

References

[1] P. Willmott, "An Introduction to Synchrotron Radiation, Techniques and Applications", John Wiley and Sons, Ltd, (2011), ISBN 978-0470.74578-6.

[2] H. Wiedemann, "Particle Accelerator Physics", 3rd ed., Springer, Berlin, Heidelberg, New York, (2007), ISBN 978-3-540-49043-2.

[3] K. Wille, "The Physics of Particle Accelerators, an introduction", Oxford University Press, (2000), ISBN 0-19-850549-3.

[4] A. Holzner, `https://en.wikipedia.org/w/index.php?curid=37948467`, 2017-03-01.

[5] Kannan M. Krishnan, "Fundamentals and Applications of Magnetic Materials", Oxford Scholarship Online, (December 2016).

[6] M. Johansson, "The MAX IV 1.5 GeV Storage Ring Magnet Design", MAX-lab Internal Note 20130712, (January 2016).

[7] Manufacturing schematic 7103016914.C, MAX IV Laboratory.

[8] The MAX IV Facility, "Detailed Design Report".

[9] J. Björklund Svensson, M. Johansson, "Relative Alignment Within the MAX IV 3 GeV Storage Ring Magnet Blocks", in *Proceedings of IPAC2015*, Richmond, VA, USA, (2015).

[10] Manufacturing schematic 7103018325.B, MAX IV Laboratory.

[11] Manufacturing schematic 725-10-01c-flange-bpm_1, MAX IV Laboratory.

[12] Manufacturing schematic 725-10-30-01d-bpm_1, MAX IV Laboratory.

[13] G. Portmann, J. Corbett, and A. Terebilo, "An accelerator control middle layer using Matlab", in *Proceedings of 2005 Particle Accelerator Conference*, (2005).

[14] `http://www.tango-controls.org/`

[15] A. Terebilo, "Accelerator modeling with Matlab Accelerator Toolbox", in *Proceedings of 2001 Particle Accelerator Conference*, (2001).

[16] J. Safranek, G. Portmann, A. Terebilo, and C. Steier, "Matlab-based LOCO", in *Proceedings of EPAC 2002*, (2002).

[17] J. Safranek, "Linear Optics From Closed Orbits (LOCO): An Introduction", USPAS June 23-27, 2003.

[18] J Safranek, "Experimental determination of storage ring optics using orbit response measurements", in *Nuclear Inst. and Methods in Physics Research, A 388(1997):27-36*, (1997).

[19] A. Kisiel, A. I. Wawrzyniak, M. B. Jaglarz, M. Kopeć, S. Piela, M. J. Stankiewicz, "Beta Function Measurement in the SOLARIS Storage Ring", National Synchrotron Radiation Centre at Jagiellonian University, Krakow, Poland, (2017).

[20] M. Sjöström, personal correspondence.

Appendices

A - Response Matrices

Linear Response Matrix

The betatron and dispersion functions are only two of many optical functions describing an optical lattice. Assume that we have n optical functions, f_1, f_2, ..., f_n, in a lattice with $m \geq n$ quadrupoles of strengths k_1, k_2, ..., k_m. Each optical function depends on each of the quadrupoles, meaning that in order to get the desired optical functions of a lattice all the quadrupole strengths have to be adjusted.

Assume the initial optical function values $\boldsymbol{F}_0 = (f_{1,0}, f_{2,0}, ..., f_{n,0})$, and the ideal values $\boldsymbol{F}_{\text{ideal}} = (f_{1,\text{ideal}}, f_{2,\text{ideal}}, ..., f_{n,\text{ideal}})$ we can expand the first order difference between the two[3]:

$$\begin{aligned}
f_{1,\text{ideal}} - f_{1,0} &= \frac{\partial f_1}{\partial k_1}(k_1 - k_{1,0}) + \frac{\partial f_1}{\partial k_2}(k_2 - k_{2,0}) + ... + \frac{\partial f_1}{\partial k_m}(k_m - k_{m,0}) \\
f_{2,\text{ideal}} - f_{2,0} &= \frac{\partial f_2}{\partial k_1}(k_1 - k_{1,0}) + \frac{\partial f_2}{\partial k_2}(k_2 - k_{2,0}) + ... + \frac{\partial f_2}{\partial k_m}(k_m - k_{m,0}) \\
&\vdots \\
f_{n,\text{ideal}} - f_{n,0} &= \frac{\partial f_n}{\partial k_1}(k_1 - k_{1,0}) + \frac{\partial f_n}{\partial k_2}(k_2 - k_{2,0}) + ... + \frac{\partial f_n}{\partial k_m}(k_m - k_{m,0})
\end{aligned} \tag{8.1}$$

where $\boldsymbol{K}_0 = (k_{1,0}, k_{2,0}, ..., k_{m,0})$ are the initial quadrupole strengths and $\boldsymbol{K} = (k_1, k_2, ..., k_m)$ are the corrected strengths.

Equation (8.1) can be written in matrix form:

$$\begin{pmatrix} f_{1,\text{ideal}} \\ f_{2,\text{ideal}} \\ \vdots \\ f_{n,\text{ideal}} \end{pmatrix} - \begin{pmatrix} f_{1,0} \\ f_{2,0} \\ \vdots \\ f_{n,0} \end{pmatrix} = \begin{pmatrix} \frac{\partial f_1}{\partial k_1} & \frac{\partial f_1}{\partial k_2} & ... & \frac{\partial f_1}{\partial k_m} \\ \frac{\partial f_2}{\partial k_1} & \frac{\partial f_2}{\partial k_2} & ... & \frac{\partial f_2}{\partial k_m} \\ \vdots & \vdots & \ddots & \vdots \\ \frac{\partial f_n}{\partial k_1} & \frac{\partial f_n}{\partial k_2} & ... & \frac{\partial f_n}{\partial k_m} \end{pmatrix} \cdot \begin{pmatrix} k_1 - k_{1,0} \\ k_2 - k_{2,0} \\ \vdots \\ k_m - k_{m,0} \end{pmatrix} \tag{8.2}$$

$$\boldsymbol{F}_{\text{ideal}} - \boldsymbol{F}_0 = \mathbf{A}(\boldsymbol{K} - \boldsymbol{K}_0)$$

The matrix **A** is known as the linear response matrix. It contains the linear response of the lattice[3].

Orbit Response Matrix

The orbit response matrix gives the relation between the strengths of the dipole corrector kicks and the change in closed orbit. This can be derived in the same manner as the linear response matrix, but each function f_n is the orbit displacement at a given longitudinal position of the ring. The effect of a series of dipole kicks on the beam displacement is given by[2]:

$$x(s) = \frac{\sqrt{\beta(s)}}{2\sin(\pi\nu)} \sum_i \sqrt{\beta_i}\theta_i \cos\Big(\nu(\psi(s) - \psi_i + \pi)\Big) \tag{8.3}$$

Given a change in dipole kick, $\Delta\theta_i$, of the i:th dipole corrector the corresponding change in beam displacement, $\Delta x(s_j) = \Delta x_j$, at a longitudinal position s_j is given by:

$$\Delta x_j = \frac{\sqrt{\beta_i\beta_j}}{2\sin(\pi\nu)} \Delta\theta_i \cos\Big(\nu(\psi_j - \psi_i + \pi)\Big) \tag{8.4}$$

In a similar way to Equation (8.1) the first order difference between the initial and the ideal orbit can be expanded:

$$\begin{aligned}
x_{1,\text{ideal}} - x_{1,0} &= \frac{\partial x_1}{\partial\theta_1}(\theta_1 - \theta_{1,0}) + \frac{\partial x_1}{\partial\theta_2}(\theta_2 - \theta_{2,0}) + ... + \frac{\partial x_1}{\partial\theta_m}(\theta_n - \theta_{m,0}) \\
x_{2,\text{ideal}} - x_{2,0} &= \frac{\partial x_2}{\partial\theta_1}(\theta_1 - \theta_{1,0}) + \frac{\partial x_2}{\partial\theta_2}(\theta_2 - \theta_{2,0}) + ... + \frac{\partial x_2}{\partial\theta_m}(\theta_m - \theta_{m,0}) \\
&\vdots \\
x_{n,\text{ideal}} - x_{n,0} &= \frac{\partial x_n}{\partial\theta_1}(\theta_1 - \theta_{1,0}) + \frac{\partial x_n}{\partial x_2}(\theta_2 - \theta_{2,0}) + ... + \frac{\partial x_n}{\partial\theta_m}(\theta_m - \theta_{m,0})
\end{aligned} \tag{8.5}$$

here x_i is only the horizontal orbit displacement. The θ_i are either the horizontal or the vertical correctors depending on whether the horizontal or coupled orbit response is to be found.

As in the case of the linear response matrix the orbit response is now put into matrix form:

$$\begin{pmatrix} x_{1,\text{ideal}} \\ x_{2,\text{ideal}} \\ \vdots \\ x_{n,\text{ideal}} \end{pmatrix} - \begin{pmatrix} x_{1,0} \\ x_{2,0} \\ \vdots \\ x_{n,0} \end{pmatrix} = \begin{pmatrix} \frac{\partial x_1}{\partial\theta_1} & \frac{\partial x_1}{\partial\theta_2} & \cdots & \frac{\partial x_1}{\partial\theta_m} \\ \frac{\partial x_2}{\partial\theta_1} & \frac{\partial x_2}{\partial\theta_2} & \cdots & \frac{\partial x_2}{\partial\theta_m} \\ \vdots & \vdots & \ddots & \vdots \\ \frac{\partial x_n}{\partial\theta_1} & \frac{\partial x_n}{\partial\theta_2} & \cdots & \frac{\partial x_n}{\partial\theta_m} \end{pmatrix} \cdot \begin{pmatrix} \theta_1 - \theta_{1,0} \\ \theta_2 - \theta_{2,0} \\ \vdots \\ \theta_m - \theta_{m,0} \end{pmatrix} \tag{8.6}$$

$$\boldsymbol{X}_{\text{ideal}} - \boldsymbol{X}_0 = \mathbf{A}_{xx}(\boldsymbol{\theta} - \boldsymbol{\theta}_0)$$

here $\boldsymbol{X}_{\text{ideal}}$ and $\boldsymbol{X}_0$ are vectors containing the horizontal orbit displacements at n longitudinal positions throughout the ring. Not to be confused with $X = (x, x')$,

which is a vector containing the horizontal displacement and displacement angle of a single particle.

The same derivation can be done for the vertical and coupled orbit response matrices. The full orbit response matrix is then given by:

$$\mathbf{A} = \begin{bmatrix} \mathbf{A}_{xx} & \mathbf{A}_{xy} \\ \mathbf{A}_{yx} & \mathbf{A}_{yy} \end{bmatrix} \tag{8.7}$$

The orbit response matrix is used, for instance, when correcting the orbit in a storage ring.

B - Sliced AT Magnets

The following tables contain the field distributions of the sliced magnets in the AT model.

	Quadrupole Field [T/m]	Sextupole Field [T/m^2]	length [m]
`sqfi_en`	5.020906	26.461865	0.05
`sqfi_m`	4.994406	29.107157	0.15

Table 8.1: Field distribution of sliced SQFI magnets in the AT model. The two slices are also mirrored so that the complete magnet consists of four slices.

	Quadrupole Field [T/m]	Sextupole Field [T/m^2]	length [m]
`sqfo_en`	5.856492	42.698155	0.05
`sqfo_m`	5.731083	45.143170	0.10
`sqfo_ex`	5.621627	42.455760	0.05

Table 8.2: Field distribution of sliced SQFO magnets in the AT model.

	Bending Angle [°]	Quadrupole Field [T/m]	length [m]
bm14	0.000618	0.008343	0.020
bm13	0.000961	0.009207	0.025
bm12	0.015292	−0.024327	0.025
bm11	0.125509	−0.423104	0.025
bm10	0.247455	−0.888986	0.025
bm9	0.355127	−1.368367	0.025
bm8	0.375371	−1.350057	0.025
bm7	0.375563	−1.348422	0.025
bm6	0.375563	−1.349049	0.025
bm5	0.375546	−1.349658	0.025
bm4	0.375511	−1.349618	0.025
bm3	0.375466	−1.349474	0.025
bm2	1.501279	−1.349420	0.100
bm1	1.500399	−1.348768	0.100
bm0	1.499896	−1.348430	0.100
b0	1.499930	−1.348404	0.100
b1	1.500490	−1.348832	0.100
b2	1.501451	−1.349520	0.100
b3	0.375514	−1.349640	0.025
b4	0.375563	−1.349897	0.025
b5	0.375597	−1.349614	0.025
b6	0.375617	−1.349287	0.025
b7	0.375620	−1.348628	0.025
b8	0.375428	−1.350422	0.025
b9	0.355190	−1.369738	0.025
b10	0.247507	−0.889982	0.025
b11	0.125543	−0.422443	0.025
b12	0.015355	−0.020128	0.025
b13	0.000978	0.009392	0.025
b14	0.000661	0.008580	0.020

Table 8.3: Field distribution of sliced dipole bending magnets in the AT model.

C - Magnet Resistances

The following main coil and shunt resistances were measured using the procedure described in Section 5.3.

Magnet #	Main Coil [Ω]	Shunt [Ω]
1	0.02449	2.43
2	0.02452	2.28
3	0.02456	2.32
4	0.02476	2.42
5	0.02465	2.51
6	0.02474	2.32
7	0.02471	2.30
8	0.02449	2.44
9	0.02448	2.30
10	0.02476	2.49
11	0.02459	2.45
12	0.02465	2.31

Table 8.4: Main coil and shunt resistances of the SQFI magnet family.

Magnet	Main Coil [Ω]	Shunt [Ω]
1	0.02555	2.55
2	0.02505	2.54
3	0.02506	2.37
4	0.02480	2.39
5	0.02513	2.39
6	0.02517	2.37
7	0.02522	2.48
8	0.02520	2.51
9	0.02496	2.60
10	0.02500	2.61
11	0.02534	2.41
12	0.02539	2.41
13	0.02548	2.36
14	0.02561	2.37
15	0.02528	2.52
16	0.02574	2.52
17	0.02488	2.34
18	0.02442	2.36
19	0.02521	2.50
20	0.02510	2.54
21	0.02471	2.52
22	0.02503	2.55
23	0.02467	2.41
24	0.02506	2.37

Table 8.5: Main coil and shunt resistances of the SQFO magnet family.

Magnet #	Main Coil [Ω]
1	0.01327
2	0.01316
3	0.01316
4	0.01316
5	0.01314
6	0.01310
7	0.01324
8	0.01320
9	0.01307
10	0.01308
11	0.01313
12	0.01315
13	0.01309
14	0.01312
15	0.01319
16	0.01312
17	0.01322
18	0.01316
19	0.01311
20	0.01313
21	0.01317
22	0.01321
23	0.01321
24	0.01326

Table 8.6: Main coil resistances of the DIP magnet family.

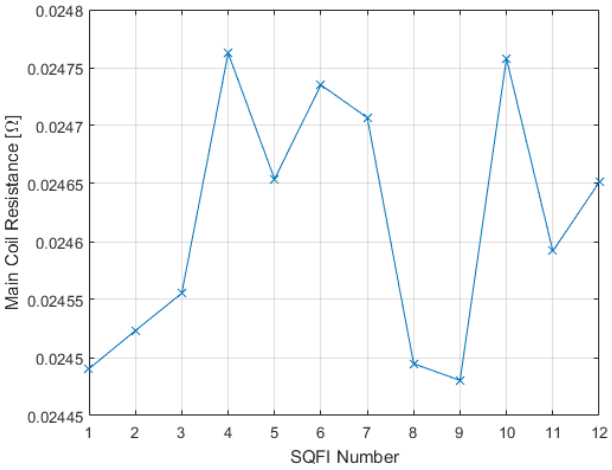

(a) Main coil resistances.

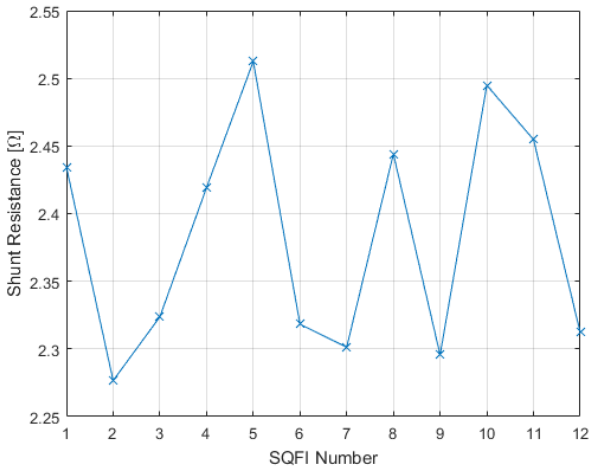

(b) Shunt resistances.

Figure 8.1: Main coil and shunt resistances of SQFI magnets (see Table 8.4).

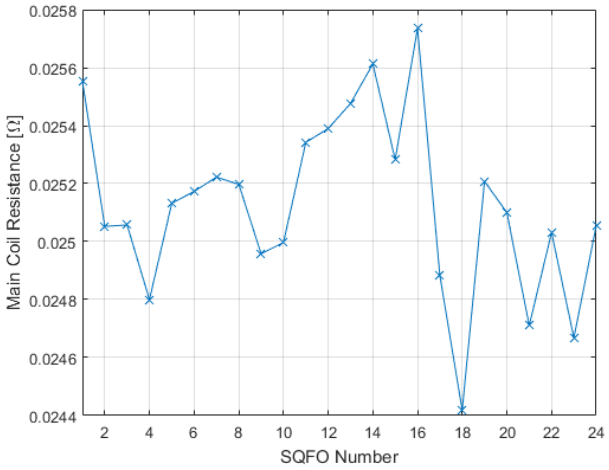

(a) Main coil resistances.

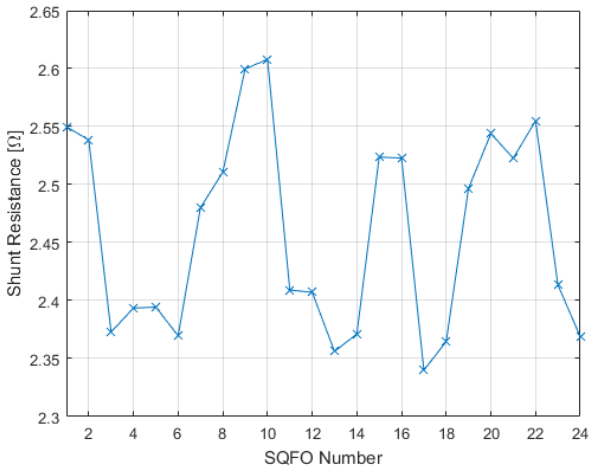

(b) Shunt resistances.

Figure 8.2: Main coil and shunt resistances of SQFO magnets (see Table 8.5).

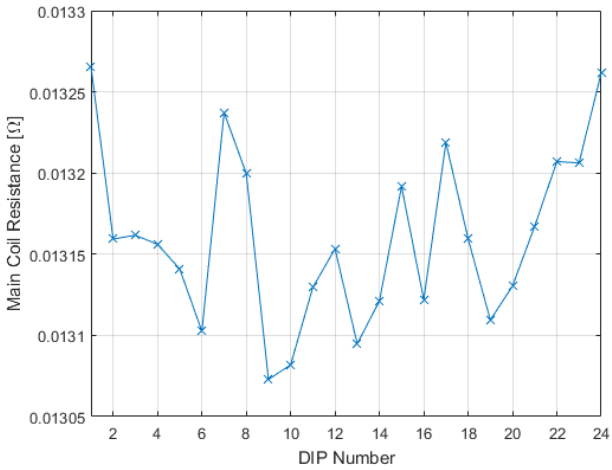

Figure 8.3: Main coil resistances of DIP magnets (see Table 8.6)

Printed by Tryckeriet i E-huset, Lund 2017

LUND
UNIVERSITY

Series of Master's theses
Department of Electrical and Information Technology
LU/LTH-EIT 2017-582

http://www.eit.lth.se